Environ Monit Assess (2022) 194:557
https://doi.org/10.1007/s10661-022-10227-0

Geotechnologies as decision support strategies for the identification of fire-susceptible areas in Rio de Janeiro State

Leandro de Souza Camargo · Corbiniano Silva · Luiz Claudio Gomes Pimentel · Rodrigo Werner da Silva · Marco Antonio Basques Sobrinho · Luiz Landau

Received: 10 November 2021 / Accepted: 20 June 2022

Abstract Forest fires have global, regional, and local socioeconomic and environmental consequences, with negative effects on ecosystem services, air quality, population health, and other relevant aspects, emphasizing their significance in the context of the United Nations Sustainable Development Goals. The study identified areas in the Rio de Janeiro State (RJS) with varying degrees of susceptibility to fire focis using remote sensing data derived from topographic, anthropogenic, meteorological, and hydrological factors based on seasonality and integrated into geographic information systems. The analytical hierarchy process was used as a method of integration and normalized hierarchy of variables, generating susceptibility maps in the annual, summer, and winter periods in the RJS's hydrographic regions (HR), with the application of the associated chi-square test to records of fire focis from the AQUA satellite, period 2003 to 2017, without methodological variation for data acquisition, whose susceptibility was classified as very low to very high. The results show that the years with the most fire foci in the adopted time series are 2007 and 2014, with a peak in September and a fall from October onwards. According to the susceptibility map, 9% of the RJS is highly susceptible during the annual period, with HR-IX being especially vulnerable. In the summer, 0.2% of RJS is extremely vulnerable, while 32% is highly vulnerable in the winter, with 6402 km^2 of HR-IX areas being extremely vulnerable. A statistical correlation was discovered between the chi-square test and susceptible areas. This work contributes as a decision-making tool in fire planning and emergency response, with the potential to assist control bodies (city halls, civil defense, environmental protection bodies, health systems) in the local and regional context in the assessment, analysis, and management of these phenomena.

Keywords Fire risk · Fire foci · Susceptibility · AHP · GIS · SDGs

L. de Souza Camargo · R. W. da Silva
State Center for Natural Disasters Monitoring and Alerting (CEMADEN - RJ), Rio de Janeiro, Brazil
e-mail: leoscamargof5@gmail.com

R. W. da Silva
e-mail: werner.rodrigo@gmail.com

L. de Souza Camargo · L. C. G. Pimentel
Graduate Program in Meteorology, Federal University of Rio de Janeiro, Rio de Janeiro, Brazil
e-mail: luizpimentel@igeo.ufrj.br

L. de Souza Camargo · M. A. B. Sobrinho
Janeiro Fire Department (CBMERJ), Rio de , Brazil
e-mail: basques_marco@hotmail.com

C. Silva (✉) · L. Landau
Civil Engineering Program, Federal University of Rio de Janeiro, Rio de Janeiro, Brazil
e-mail: corbiniano@gmail.com

L. Landau
e-mail: landau@lamce.coppe.ufrj.br

Published online: 04 July 2022

Introduction

Fire affects of the Earth's surface, burning an average of 363.41×10^6 ha of the planet's total area from 2015 to 2019 (Wei et al., 2021). It integrates the geological cycle and rural culture and influences the biodiversity, soil properties, the carbon cycle, sediment and water production, air and water pollution, as well as all associated risks, aspects, and characteristics that necessitate planning, organization, and decision-making for its management (Cerdà, 2020).

According to Bowman et al. (2020), factors such as fire behavior, size, frequency, intensity, severity, seasonality of burning, and other complexities describe the components of fire regimes and determine the gasses and aerosols, and particulates released into the atmosphere (Majdi et al., 2019; Palm et al., 2020). Among the fires' negative effects are water supply and air quality impacts and changes in the land surface and precipitation patterns, which can cause desertification (Nunes et al., 2018).

Fires are distinguished by their extent, speed, and potential to affect fauna, flora, the local economy, and the population (Dickman, 2021), with socioeconomics and health consequences (Wunder et al., 2021). In Brazil, the primary cause of fires is typically related to human activities, including burning for agricultural activities, clearing pasture areas, and wood extraction (Oliveira et al., 2020; Santos et al., 2021).

Fires continue to be a significant natural disturbance in many ecosystems, helping to shape biome distributions, control the carbon balance, and influence terrestrial carbon cycling and significant changes, with serious consequences for human societies and security risks (Wu et al., 2021). Its primary causes and consequences are related to natural factors (Aragão et al., 2007; Chandler, 1982; Corcoran et al., 2011; Littell et al., 2016; Rorig & Ferguson, 1999), and Human factors (Altay et al., 2013; Badia et al., 2019; Bowman et al., 2020; Cardil & Molina, 2015; Cardil et al., 2020; Kiely et al., 2021; Pereira et al., 2021; van Mantgem et al., 2015).

Fire and its consequences have a direct impact on nine of the seventeen proposed United Nations Sustainable Development Goals – SDGs (UNEP, 2021) related to geographic expansion, environmental quality, climate change, and land use (Martin, 2019). Fire provides insights and guidance for implementing various SDGs such as environmental protection; emissions with regional and global impacts on air quality, precipitation, and greenhouse gas contribution to global warming: carbon dioxide (CO_2) and black carbon (Haines et al., 2017; Lowe & Bernie, 2018); its role in the global process of land degradation (UN, 2015; Hill et al., 2018); as well as its impact on ecosystem services such as air and water quality, precipitation, and soil patterns; it is also linked to seven SDGs (Martin, 2019).

All of the risks, aspects and characteristics associated with fires necessitate planning, organization, and decision-making. In this way, fires necessitate firefighting and management strategies that use increasingly effective methods. From this perspective, the use of tools that geographically represent fire-prone areas is critical in the investigation of the factors that promote its emergence. These tools can help with land use and protected area management, reducing and mitigating the harmful effects of fires and contributing to decision-making processes and planning actions aimed at predicting and preventing these occurrences.

Remote sensing (RS) is essential for the identification, evaluation, and analysis of these phenomena. According to Pettinari and Chuvieco (2020), satellite observations provide significant resources for the evaluation of several variables that integrate fires: ignition sources, fuel state and abundance, topography and meteorological conditions that influence fire propagation, and so on. This data is useful for estimating, with a focus on global and continental fire risk systems, as well as providing near real-time information about fire occurrences for preventive response teams. Adab et al. (2021) developed a fire probability index based on the efficiency and effectiveness of satellite imagery early warning systems in fire prevention and mitigation, making it a useful tool for decision-making in fire management in near real time.

Geographic information systems (GIS) applications relevant to spatial, geobiophysiographic, and socio-environmental analysis can support practical and low-cost solutions, improve results, and be used to integrate analyses, particularly in areas prone to fires, where soil, topography, and climatology can be used as influencing factors. Tehrany et al. (2019) used the LogitBoost ensemble-based decision tree machine learning method to map wildfire susceptibility in Vietnam, and the results can accurately predict

wildfire-prone areas, potentially with applications in forest conservation management. Eslami et al. (2021) created forest fire susceptibility maps in Iran using random forestry methods, artificial neural networks, and logistic regression models. Abedi Gheshlaghi (2019) created wildfire risk maps in northern Iran using GIS-based multi-criteria decision analysis (MCDA). Sivrikaya and Küçük (2022) created risk maps for forest fires in Turkey using GIS-MCDA, the analytical hierarchy process (AHP), and the statistical index (SI). Srivastava et al. (2019) identified areas in India with high severity and probability of wildfires using the normalized burn rate calculated from Landsat TM5 data. The multi-criteria assessment attributes allow for the prediction of fire-prone areas. Ager et al. (2021) used fire risk reduction models in 76 national forests (58 million ha) across 15 western and central US states. ForSys was used to recover affected areas, and FSim was used to simulate large-scale fires. In analyzing and communicating forest fire management initiatives, the methods emphasize the use of scenario planning. Leuenberger et al. (2018) used non-linear methods to map wildfire susceptibility in a highly vulnerable region of Portugal, comparing extreme learning machine and random forest stochastic approaches to a deterministic method based on the location of pixels with similar standardized susceptibility and total burned area. Bergonse et al. (2021) evaluated the prevention of potential burned areas in Portugal before the critical fire season, using logistic regression models that combine susceptibility to forest fires with the meteorological index. The model can help with resource optimization and allocation for prevention, early detection, and suppression activities.

Multi-criteria analysis methodologies are used to seek optimized solutions from the investigation of problem-solving alternatives by Castro et al. (2015). It is based on the spatial modeling of various criteria for selecting suitable areas through different concepts: restriction, a legal issue criterion associated with the impossibility of changing the environment in specific locations; and adequacy, a scale of values that represents the greatest adjustment of a given area in relation to another. The process is carried out using weights and the AHP methodology, which was developed and consolidated by Saaty (1977) and is widely used in the scientific literature (Kumari & Pandey, 2020; Nuthammachot & Stratoulias, 2021). The AHP compares the importance in pairs, with all factors implicitly ordered to reduce arbitrariness and eventual inconsistencies in determining their weights, and its development process evaluates the consistency of the comparison, indicating whether or not it is random (Castro et al., 2015; Lorentz et al., 2016).

Several studies depict fires in the Rio de Janeiro State (RJS). Gois et al. (2020) assessed the spatio-temporal variability of fire foci in the RJS, as well as the environmental and socioeconomic characteristics critical to their dynamics, using statistical procedures (descriptive, exploratory, and multivariate analyses) and data from environmental satellites. Behling et al. (2020) investigated the links between climate and fire processes and ecological patterns in the mid and late Holocene (4870 years BP) in Serra de Itatiaia, RJS. Freitas et al. (2020) investigated how fire focis distribution influences the spatio-temporal vegetation cover pattern in the RJS using fire foci, the Enhanced Vegetation Index (EVI) from the MODIS sensor, and Kernel density calculations.

Estimating the likelihood of a fire and associating it with environmental and human conditions is an important step in supporting forest protection plans, contributing to the reduction of its consequences and assisting in emergency planning actions. The goal of this article is to identify the RJS regions that have different hierarchical levels of susceptibility to the occurrence of fires, thereby subsidizing the planning and management policies of local environmental agencies in response to the problem.

Materials and methods

Study area

Rio de Janeiro State, located in Southeast Brazil (SEB), has a territorial area of 43,750.427 km^2, with a population of 17,264,943 and a demographic density of 394.62 inhabitants/m^2 (IBGE, 2021). It has nine hydrographic regions (HRs): I (Baía da Ilha Grande), II (Guandu), III (Médio Paraíba do Sul), IV (Piabanha), V (Baía de Guanabara), VI (Lagos São João), VII (Rio Dois Rios), VIII (Macaé e das Ostras), and IX (Baixo Paraíba do Sul e Itabapoana); defined as environmental planning units, to assess the vulnerability of fire risk across the state (Fig. 1).

There are 92 municipalities in the state, which are divided into eight administrative divisions

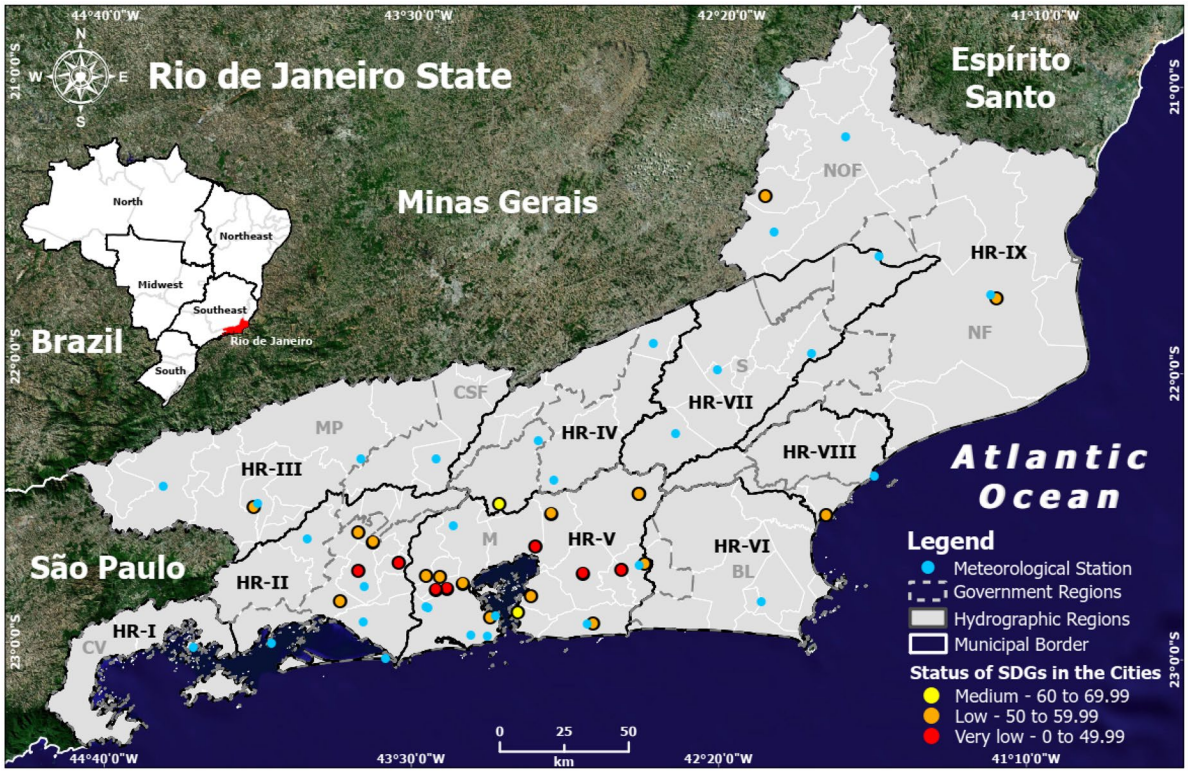

Fig. 1 Geographic setting of the study area

(government regions): Noroeste Fluminense (NOF), Norte Fluminense (NF), Baixadas Litorâneas (BL), Serrana (S), Centro-Sul Fluminense (CSF), Metropolitana (M), Médio Paraíba (MP), and Costa Verde (CV) (Fig. 1). Alvares et al. (2013) presented the climate for the state's administrative divisions based on the Köppen classification: tropical for NOF, NF, and BL; tropical monsoon for M; humid maritime climate for S; and subtropical/altitude tropical climate for MP and CSF.

The most diverse climate changes have occurred in recent decades, contributing to increased vulnerability to climate risks associated with the gradual increase in average air temperature, extreme rainfall, and, most notably, the severity and duration of droughts in some Rio de Janeiro regions (Brito et al., 2017; Sobral et al., 2018).

Most of the time, the RJS is influenced by a south Atlantic Subtropical Anticyclone (SASA), which creates clear or cloudy skies and prevailing north and northeast winds of low intensity, mainly in the state's northeast (FIDERJ, 1978). According to Reboita et al. (2010), the following transient systems in the region include extratropical cyclones, cyclonic vortexes of high subtropical origin, and mesoscale convective systems, which promote increased cloudiness, precipitation, and wind intensification. The formation of the South Atlantic convergence zone (SACZ), which is characterized by a band of convective cloudiness extending in general from the Amazon to the Atlantic Ocean in a northwest-southeast direction, is common from November to March (Kodama, 1992, 1993; Kousky, 1988).

Decades of research have shown that the RJS is characterized by high precipitation variability due to its complex topography and proximity to the coast, which influences the occurrence of mesoscale meteorological systems such as land/sea and valley/mountain breezes and mesoscale convective systems over the region (Brito et al., 2017; Davis & Naghettini, 2000; Dereczynski et al., 2009; Lima et al., 2021; Nimer, 1972).

The maximums are typical of high-altitude areas, while the minimums are typical of lowland and

coastal areas (Silva & Dereczynski, 2014; Sobral et al., 2018). The highest annual average rainfall indexes, according to Silva and Dereczynski (2014), are found on the border of the Metropolitana region and the coastal lowies with the Serrana region, where the average annual rainfall ranges between 2500 and 2800 mm. According to Brito et al. (2017), Sobral et al. (2018), and Lyra et al. (2018), total annual rainfall ranges from 1000 to 2300 mm, while Alvares et al. (2013) reported that air temperature ranges between 12 and 14 ℃ on higher altitude (> 850 m.a.s.l.) regions and between 24 and 26 ℃ on coastal regions.

According to a recent study by Sobral et al. (2018), the average annual rainfall in the Rio de Janeiro state for the period (1979–2009) was 1544 mm, which was distributed as follows: BL (2144 mm), CV (1912 mm), MP (1602 mm), M (1571 mm), and S (1547 mm) had higher averages than the state average during the period, while the CS (1307 mm), NOF (1235 mm), and NF (1033 mm) were below average. In terms of seasonality, the months with the least rain are June, July, and August, while the months with the highest rainfall totals are between November and March, depending on the region of the state.

Data and information

The list of data used includes the records of fire foci from 2002 to 2017 (from AQUA – Aqua Earth-observing satellite mission, version launched on 05/04/2002 (INPE, 2022)), from the INPE, Instituto Nacional de Pesquisas Espaciais, which saves the hourly records to the burnt database (BDQueimadas), available in https://queimadas.dgi.inpe.br/queimadas/bdqueimadas (INPE, 2021). Geobiophysiographic data, including land use and cover of the INEA, Instituto Estadual do Ambiente (INEA, 2021), the base year 2015. Geomorphological data include slope orientation, altimetry, and declivity, with a spatial resolution of 30 m (SRTM – Shuttle Radar Topography Mission), from the USGS – United States Geological Survey (USGS, 2021). Climatological data (water deficit, temperature, and precipitation), with a spatial resolution of 1 km^2 cover from 1977 to 2000 (Fick & Hijmans, 2017). ArcGIS 10.5, Excel 2013, and the R Gui statistical program were the computational platforms that supported the results preparation and respective analysis.

Methodology: identification of fire focis and susceptibility parameters

According to Fig. 2, this study is based on six integrated approaches: (1) conceptual definition, (2) obtaining and pre-processing necessary data, (3) exploratory analysis of fire foci, (4) data processing and product generation, (5) AHP method application, with the establishment of condition weights and elaboration of the susceptibility map to the occurrence of fire risk in the RJS based on the fire foci, and (6) results from validation.

The conceptual definition (1) is based on the annual identification of fires that occurred in the RJS (Aximoff et al., 2016; Fernandes et al., 2011), whose determination of its conditions, meteorological, hydrological, topographic, and anthropic factors, favors the appearance of fire foci, according to previous studies (Adab et al., 2013; Matin et al., 2017; Prudente & Rosa, 2010; Sausen & Lacruz, 2015). Contributions that emphasize the main environmental variables that trigger hot flashes are land slope, land use, temperature, precipitation, slope orientation, altimetry, and water deficit. These conditions enhance the appearance of fire foci during periods of low precipitation, which can evolve and become fires.

The spatial information (2) obtained includes climatological data from the WorldClim database (Fick & Hijmans, 2017), composed of a set of global climatic layers (climate grids), with a spatial resolution of 1 km^2. The topographic data from the SRTM with a spatial resolution of 30 m. The goal of the SRTM was to create a digital model of the land area between 56 and 60° N so that a full base of terrestrial digital topographic letters with a spatial resolution of 1 arc-second (= 30 m) could be generated. The geobiophysiographic data from the INEA (INEA, 2021) and annual and monthly fire foci records (INPE, 2021).

The identification of fire focis is carried out by ten satellites that have optical sensors operating in the average thermal range of 3.7 to 4.1 m of the optical spectrum, on board eight polar orbit satellites 18 and 19, Metop-B and C (Advanced Very High Resolution Radiometer/3 – AVHRR/3 sensor), NASA Earth and Aqua (MODIS Sensor), and NPP-Suomi (Suomi National Polar-orbiting Partnership) and NOAA-20 (Visible Infrared Imaging Radiometer Suite – VIIRS Sensor), and two geostationaires, Goes-16 (Geostationary Operational Environmental Satellite) and

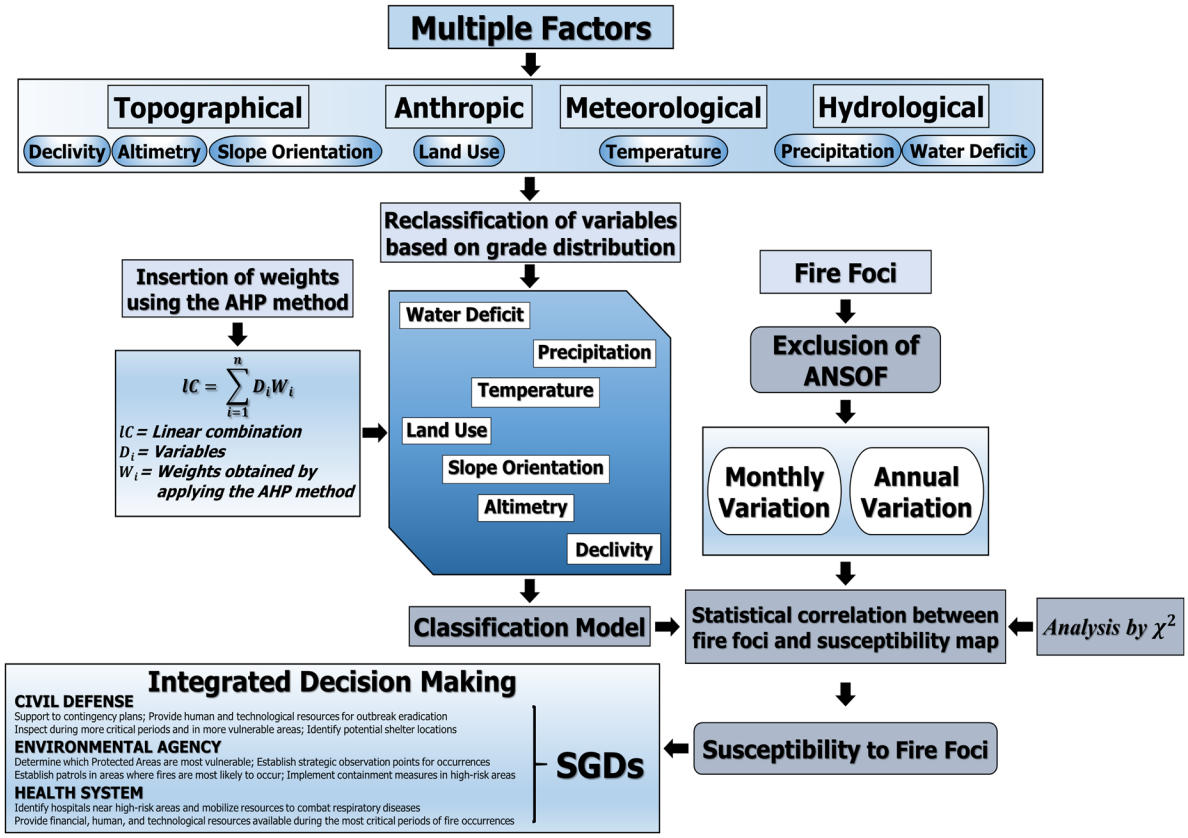

Fig. 2 Flowchart with the methodological representation of all study stages

MSG-3 (Meteosat Second Generation), where each every day, more than 100 images are analyzed specifically to detect focis of vegetation burning, and the data is freely available.

The detection of fire focis is based on the emission of infrared radiation from fires, with an algorithm that examines each pixel of the MODIS sensor, categorizing them as missing data, cloud, water, no fire, fire, or unknown (Justice et al., 2006).

The algorithm determines fire focis by using brightness temperatures derived from 4 m wavelengths (channels 21 and 22) and 11 m wavelengths (channel 31), denoted by T4 and T11, respectively. Channel 32 is used to mask clouds. Channels 1 and 2 are used to filter out false alarms and to mask clouds. Channel 7 is used to reject false detections caused by water. Pixels that do not contain valid data are immediately classified as missing or deleted data.

To determine low-intensity fires, the fire detection strategy is based on absolute fire detection and relative detection of the thermal emission of surrounding pixels. The goal of this method is to find pixels with values greater than the average thermal emission of the surrounding pixels, as well as to compute the surface temperature variation and sunlight reflection.

The analysis of the fire foci dataset (3) related to the Atlantic Forest biome was obtained from the AQUA MT satellite and considered a 14-year observation period (January 2003 to December 2017), distinguishing itself by the type of sensor (MODIS) and satellite (polar and heliosynchronous). The data were separated into annual and monthly data, representing occurrences at different times in the study region. We highlight the differentiation of outbreaks in terms of occurrence in unlikely places: water bodies, rocky outcrops, and urban areas, designated as ANSOF (areas not susceptible to the occurrence of fires), which were identified from the land use database and excluded from the time series. The seasonal

fire foci behavior was determined using boxplots on annual and monthly scales, which are useful in identifying outliers.

For data processing (4), the data were converted into a vector format (shapefile) as matrices, generating maps of land use and water deficit. According to the INEA metadata section (INEA, 2021), the construction of the land use and coverage was made from the use of Landsat-8 satellite scenes, a panchromatic multispectral sensor with a 30-m spatial resolution for the year 2015, through object-directed analysis (Geobia – geographic object-based image analysis), and made available in vector format, and scale 1/250,000. According to Cronemberger et al. (2011), the water deficit was calculated using the Thornthwaite equation (Thornthwaite, 1948), which was based on average air temperature data from Worldclim and the average photoperiod for converting medium air temperature data into evapotranspiration data Potential (ET_P). Following that, the method of Thornthwaite and Mather (1955) for generating the water balance was used in the calculation of real evapotranspiration (RE). This method estimates real evapotranspiration by taking into account the storage capacity of water in the soil due to the average depth of the roots (vegetation cover) by soil type. Water storage capacity values are for medium to advanced recovery stage vegetation: approximately 300 mm, and initial 200 mm; pasture and other cultures: 100 mm; and uneven urban: 50 mm. Urban areas and bodies of water were not taken into account. The accumulated negative values, storage rate, change rate, actual evapotranspiration, water deficit, and water surplus were calculated from these values, resulting in the water balance model (Cronemberger et al., 2011), of which the values of hydric deficit for RJS.

After matching the data format, the variables were reclassified into five different notes, ranging from very low (note 1) to very high (note 5), based on the degree of flammability of the available surface biomass (soil use and cover), solar incidence (orientation), flame spread (altitude and slope), and locations where precipitation is lower than evapotranspiration (rainfall and water deficit). Using the AHP method, each chosen variable was given a normalized hierarchical ordinal value after reclassification. The geographical coordinates were transformed into metrics using the equivalent conical projection of Albers (Oliveira & Saraiva, 2015) and estimating the area occupied by each susceptibility class in the RJS in square kilometers (Camargo et al., 2019). Data on water deficit, precipitation, and temperature have variable frequency distributions, as they reflect different seasonal periods (annual, summer, and winter). To standardize these variables, the observed values (x_i) were transformed into score values (z_i), as proposed by Ferreira (2017), using Eq. (1).

$$z_i = \frac{x_i - \overline{X}}{\sigma} \tag{1}$$

where x_i is the observed data, $\overline{X}$ is the average of observations, and σ is the standard deviation of observations.

According to Ferreira (2017), using the standard scale for data on water deficit, precipitation, and temperature can help to remove the interference of seasonal frequency variations. Negative z_i values indicate that the x_i value in the seasonal period studied is lower than the regional average; positive values indicate the opposite, that x_i is higher than the regional average; and when $z_i = 0$, x_i is equal to the seasonal average. In this regard, the standardized variable z_i is more effective at quantitatively positioning a geographical unit in relation to the regional context (Charre, 1995).

The weights establishment or degree of contribution of each conditioner is based on multi-criteria analysis through the AHP method (5), whose application includes the following: organization of the conditions in a matrix format (parallel comparison matrix); logical verification of the calculated weights matrix (eigenvector); consistency of the matrix; consistency ratio (CR), which assesses the measure of the consistency of the decision and describes the integrity or quality of the judgments. It is obtained by the ratio between the consistency index (CI), which indicates the eigenvalue deviation from an expected theoretical value n, and the random consistency index (RC), which represents the value to be obtained in an order comparison matrix n. For the determination of CR, CI was compared with RC, and the determination of the quality of the judgment was made.

Based on numerical values obtained by the AHP method application, the level of importance each conditioner exerts in fire foci occurrence, called weights, was established, which were later combined by overlapping the themes, to indicate the most vulnerable regions for which susceptibility maps were generated.

The resulting scale adopted in the overlapping of the themes at different cartographic scales was the lowest spatial resolution. In this sense, Worldclim's spatial resolution is 1 km^2, corresponding to a scale of 1/5,000,000, ensuring that positioning or geometry errors remain below those specified for the mapping scale (Moura et al., 2009; Sampaio & Brandalize, 2018), which is compatible with RJS's geographic extension.

To assess the proposed cartographic model accuracy (6), the annual records of fire foci between 2003 and 2017 were compared with the annual susceptibility map, obtaining the frequency of occurrence by susceptibility class, as well as the fire focis that appeared between December and March (Brazilian summer season) and from June to September (Brazilian winter season), represented by bar graphs. The measure of association between the variables' "susceptibility maps" and "burning events" was performed using the chi-square test (χ^2) for two independent samples, with a confidence level of 95%, assuming the following hypotheses:

- H_0: The variables are independent.
- H_1: The variables are not independent.

The χ^2 statistic aims to test the independence between a probabilistic model and a set of observed data, built from the fire foci frequency extraction in each susceptibility class (the observed frequency), and the expected behavior of the correlation between fire foci and susceptibility classes (the expected frequency) by applying Eq. (2), based on the hypothesis that there is no association between the two variable categories. If the observed and expected frequency distributions are equal, the chi-square test result is null. Thus, a low value of χ^2 indicates independence between the variables (Fávero & Belfiore, 2017).

$$\chi^2 = \sum_{i=1}^{I} \sum_{j=1}^{J} \frac{(O_{ij} - E_{ij})^2}{E_{ij}} \quad (2)$$

where O_{ij} is the number of observations in the i-th category of variable X, and in the j-th category of variable Y;E_{ij} is the expected frequency of observations in the i-th category of variable X, and in the j-th category of variable Y; I is the number of categories (lines) of variable X; and J is the number of categories (columns) of variable Y.

For this study, the calculated chi-square values (χ^2_{cal}) approximately follow a χ^2, distribution, with $(I-1)$ and $(J-1)$ degrees of freedom, respectively.

Results

Spatio-temporal analysis of fire foci

Between 2003 and 2017, 12,819 fire foci were recorded in the RJS during the day, of which 2041 were classified as ANSOF when compared to the land use map (INEA, 2021) and subsequently discarded from statistical validation, leaving 10,778 total fire foci. In the annual distribution, 2007 and 2014 were marked by the maximum values of the adopted series, highlighted by the accumulation of 1378 fire foci in 2007 (Fig. 3).

In 2014, by February, 107 fire foci events were recorded, an increase of 296% compared to the average value of observations between 2003 and 2017. In 2015, by January, 86 fire foci events were registered, an increase of 562% compared to the average number

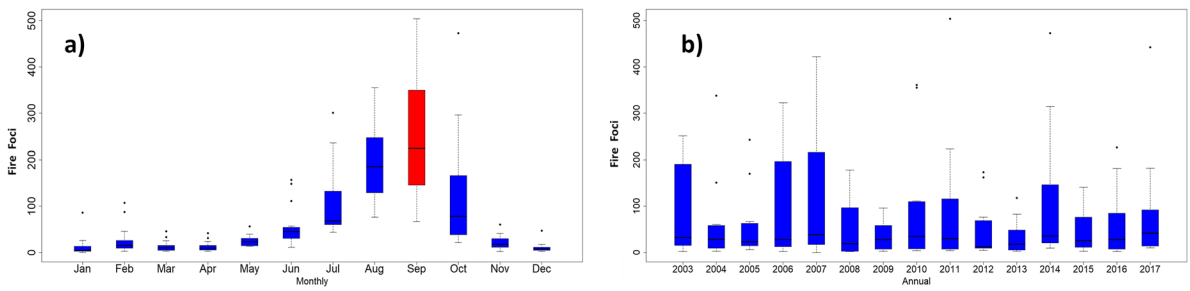

Fig. 3 Bloxplot of fire foci in RJS, 2003–2017: **a** annual and **b** monthly

of observations between 2003 and 2017. The monthly distribution of fire foci between 2003 and 2017 demonstrates the seasonal behavior of the phenomenon, showing that in January and April, the average number of fire foci remained practically stable, except for outliers, and increased in May and June. Starting in July, a progressive increase was noticed, reaching its peak in September, with a decrease in the number of records after October.

Conditioning factors

To generate the fire risk susceptibility map, seven relevant factors, including environmental variables, were considered as data for fire occurrences: topographic factors including declivity, altitude, and slope orientation (Ghorbanzadeh et al., 2018; Kolden & Abatzoglou, 2018; Lautenberger, 2017); human origin factors including land use (Pourghasemi et al., 2016); meteorological factors including temperature (annual, dry, and wet period); and hydrological factors including water deficit (annual, dry, and wet period) and precipitation (annual, dry, and wet periods) (Ganteaume et al., 2013). See Figs. 4 and 5.

Declivity

The declivity map, prepared using the SRTM digital elevation model, identified 17,829.32 km^2 with declivities classified as strongly undulating (according to EMBRAPA methodology (Santos et al., 2006)), which corresponds to 40.86% of the RJS territory. In the comparison among HRs, HR-IV (Piabanha) stands out, with 69.17% or 2452.31 km^2 with declivities greater than 45%. Table 1 highlights the susceptibility classes prevalent for each HR in relation to the declivity.

Altimetry

Using the Jenk method, which minimizes the sum of variance within each class (Ferreira, 2017), five altimetric classes were established, separated according to the highest percentage of area occupied

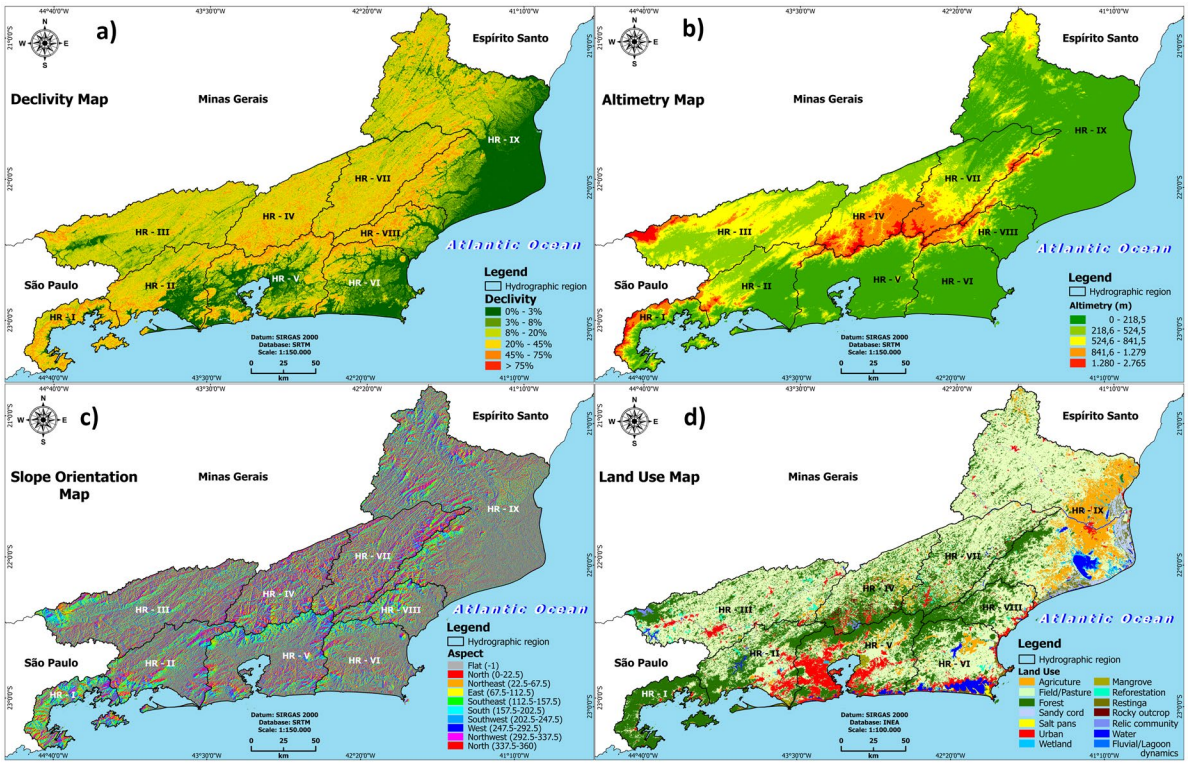

Fig. 4 Topographic factors: **a** declivity, **b** altimetry, and **c** slope orientation; human origin factors: **d** land use

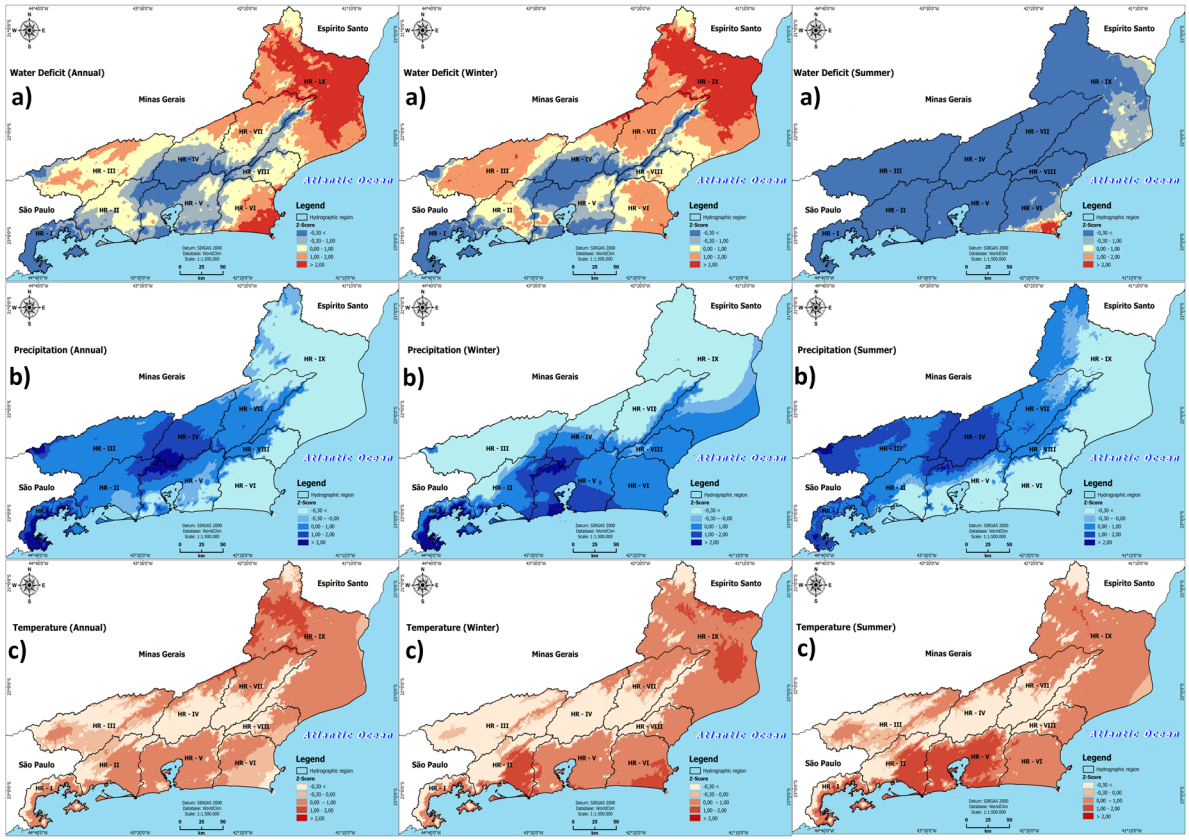

Fig. 5 Hydrological factors: **a** water deficit (annual, winter, and summer) and **b** precipitation (annual, winter, and summer); meteorological factors: **c** temperature (annual, winter, and summer)

by HRs (Table 2). The altimetric values between 1280 and 2765 m were equivalent to 3242.41 km^2 (7.43%) of the RJS. HR-I (Baía da Ilha Grande) had 346.97 km^2 (20.50%) of its occupied area with values above 1.208 m, dominating the comparison among all HRs.

Slope orientation

Slopes oriented in the N and NW directions have greater exposure to sunlight, increasing the evaporation capacity of the combustible material on the surface (Ferraz & Vettorazzi, 1998). Based on this

Table 1 Classification attributed to susceptibility category for declivity

Declivity		Note	Predominant HR		
Class	Percentage classes		Area (km^2)	Percentage	HR
Very low	0% a 3%	1	1484,55	41,22%	VI
Low	3% a 8%	2	833,69	23,15%	VI
Average	8% a 20%	3	243,81	37,86%	III
High	45% a 75%	4	1939,27	54,70%	IV
Very high	>75%	5	513,04	14,47%	IV

Table 2 Classification of susceptibility to the altimetry category

Altimetry		Note	Predominant HR		
Class	Altimetric classes		Area (km^2)	Percentage	HR
Very low	0–218.5 m	1	4431.69	32.86%	IX
Low	218.6–524.5 m	2	833.69	23.15%	VI
Average	524.6–841.5 m	3	2431.82	37.86%	III
High	841.6–1279 m	4	1939.27	54.70%	IV
Very high	1280–2765 m	5	346.97	20.50%	I

principle, the highest scores were attributed to the directions that received the most solar radiation, while directions with the least exposure received the lowest scores in the reclassification (Table 3), which occupied 24.67% of the RJS territory, equivalent to one area of 10,784.72 km^2. HR-VII (Rio Dois Rios) had 1210.08 km^2 or 27.69% of the slopes oriented in the north–northwest direction.

Land use

From land use mapping, different biomasses were identified in the RJS, whose categories and percentages of occupied area are described in Table 4 and are considered as the main contributors to the appearance of fire foci, consistent with the national and international scientific literature (Chuvieco & Congalton, 1989; Ferraz & Vettorazzi, 1998; Sausen & Lacruz, 2015). ANSOF distributed in HRs totaled 4959.32 km^2. The classes identified as "very low" and "low" dominated in HRs II, III, V, VI, and IX, totaling 645.41 km^2. Approximately 52% of the RJS consists of fields/pastures, a dominant category in HR-III (Médio Paraíba do Sul), HR-VII (Rio Dois Rios), and HR-IX (Baixo Paraíba do Sul e Itabapoana), regions with more than 50% of their area comprised of this biomass.

Water deficit

The standardization of water deficit values in the annual, summer, and winter cycles was performed using Eq. (1), for an average (μ) = 77.23 mm and standard deviation (σ) = 48.12 mm annually; (μ) = 6.44 mm and (σ) = 8.33 mm in summer; and (μ) = 56.7 mm and (σ) = 24.42 mm in winter; values were reclassified according to the deviation from the null value (average of observations) according to Table 5.

In the annual period, 1502.48 km^2 or 3% of the RJS experienced a water deficit greater than 2 standard deviations, with an interval between 173.6 and 324 mm. When comparing the HRs, HR-VI (Lagos–São João) obtained the highest percentage of the classified area above 2 standard deviations, corresponding to 422.6 km^2, or 12% of its area.

In the summer, 198.56 km^2 or 0.4% of the RJS had a water deficit greater than 2 standard deviations, with an interval between 24 and 120 mm. In the comparison between the HRs, HR-VI (Lagos–São João) obtained the highest percentage of the area classified above 2 standard deviations, corresponding to 198 km^2, or 5% of its area.

In the winter period, 250 km^2 or 1% of the RJS had a water deficit greater than 2 standard deviations, with an interval between 120 and 130 mm. In the comparison between the HRs, HR-IX (Baixo Paraíba

Table 3 Classification of susceptibility for the slope orientation category

Slope orientation		Note	Predominant HR		
Class	Exposition		Area (km^2)	Percentage	HR
Very low	Plan–south–south-east	1	631.29	36.80%	I
Low	South-west	2	749.01	11.66%	III
Average	East–west	3	1509.10	23.49%	III
High	Northeast	4	742.97	17.00%	VII
Very high	North–northwest	5	1210.08	27.69%	VII

Table 4 Classification of susceptibility for the biomass category

Class	Biomass category	Note	Predominant HR									
			Area (km^2)			Percentage			HR			
ANSOF	Water, rocky outcrop, sandy cords and dunes, urban occupation, salt flats, exposed soil	-	4959.32			11%			-			
Very low	Reforestation, mangrove	1	72.89	114.72	105.78	2%	2%	2%	II	III	V	
Low	Relic community, restinga	2	54.70	297.32		2%	2%		VI	IX		
Average	Secondary vegetation in early stage	3	437.82			10%			VII			
High	Agriculture, secondary vegetation in medium-advanced stage	4	1462.49			85%			I			
Very high	Field-pasture	5	4451.58			69%			III			

Table 5 Classification of susceptibility to the water deficit category

Class	Z-score	Water deficit (mm)	Note	Predominant HR				
				Area (km^2)	Percentage	HR		
Annual								
Very low	< −0.3	4–62.8	1	1730.84	100%	I		
Low	−0.3–0	62.81–77.23	2	3051.19	48%	III		
Average	0–1	77.24–125.3	3	1876.19	43%	VII		
High	1–2	125.4–173.5	4	5445.13	40%	IX		
Very high	> 2	173.6–324	5	422.59	12%	VI		
Summer								
Very low	< −0.3	4	1	19,781.87	100%	I	II	III
						IV		VII
Low	−0.3–0	4.1–6.4	2	2786.60	21%	IX		
Average	0–1	6.5–15	3	568.36	4%	IX		
High	1–2	16–23	4	77.50	2%	VI		
Very high	> 2	24–120	5	198	5%	VI		
Winter								
Very low	< −0.3	5–49	1	1730.84	100%	I		
Low	−0.3–0	50–57	2	680	35%	VIII		
Average	0–1	58–81	3	4236	67%	III		
High	1–2	82–110	4	6555	49%	IX		
Very high	> 2	120–130	5	248	2%	IX		

do Sul e Itabapoana) obtained the highest percentage of the classified area above 2 standard deviations, corresponding to 248 km^2, or 2% of its area.

Precipitation

The WorldClim climatological database spans the years 1970 to 2000, which is incompatible with the temporal availability of data on fire foci. In this regard, the hotspot records obtained from the AQUA satellite's MODIS sensor are critical in demonstrating the accuracy of the cartographic model developed in this study.

We compared observed precipitation and temperature data from the Climatological Normals, years 1961–1990 and 1981–2010 (INMET, 2022), recorded in different meteorological stations: 7 for precipitation and 6 for temperature; with estimated WorldClim data (1970–2000) to assess the reliability of the data used in the construction of the climatological maps. The hypothesis of data correlation was confirmed using the statistical application F of Fischer – Snedecor (with $\alpha = 0.05$ for 1 and 10 degrees of freedom). After confirming the normality of the observed and estimated data with the Shapiro–Wilk test, the Pearson test was used to determine the homoscedasticity (same finite variance) and the absence of outliers, as well as the intensity of the correlation (R) and the adjustment between the observed and estimated variables (R^2) of the sample. The results show an F-calculated of 4.96, demonstrating the correlation between the databases, distinguishing between intensity (R) and sample adjustment (R^2) (Table 6). The comparative values demonstrate database compatibility, allowing WorldClim data to be used in the representation of the meteorological variables used.

The standardization of pluviometric accumulations in the annual, summer, and winter cycles was carried out by applying Eq. (1), for an average (μ) = 1325.55 mm and standard deviation (σ) = 227.84 mm annually; (μ) = 595.59 mm and (σ) = 129.65 mm in summer; and (μ) = 102.51 mm and (σ) = 31.81 mm in winter. Values were reclassified according to the deviation from the null value (average of observations) according to Table 7.

In the annual period, 17,992 km^2 or 41% of the RJS presented accumulated precipitation less than −0.3 standard deviations, estimated between 813.6 and 1257 mm. In the comparison between the HRs, RH-VI (Lagos–São João) obtained the highest

Table 6 Statistical correlation between the Climatological normals and WorldClim databases

Stations	Climatological normals (1961–1990) and WorldClim (1970–2000)			Climatological normals (1981–2010) and WorldClim (1970–2000)		
	F-calculated	*R*	R^2	*F*-calculated	*R*	R^2
Precipitation						
Alto da Boa Vista	30,50	0,87	0,75	7,54	0,66	0,43
Campos	57,97	0,92	0,85	114,13	0,96	0,92
Carmo	210,29	0,97	0,95	293,28	0,98	0,97
Cordeiro	55,64	0,92	0,85	227,83	0,98	0,96
Itaperuna	92,44	0,95	0,9	278,57	0,98	0,97
Resende	468,92	0,99	0,98	310,92	0,98	0,97
Santa Maria Madalena	120,44	0,96	0,92	226,96	0,98	0,96
Temperature						
Campos	714,4	0,99	0,98	567,37	0,99	0,98
Cordeiro	52,76	0,92	0,84	55,23	0,92	0,84
Ecologia Agrícola	239,85	0,98	0,96	243,07	0,98	0,96
Itaperuna	53,82	0,92	0,84	88,26	0,93	0,89
Resende	930,97	0,99	0,98	330,15	0,98	0,97
Santo Antônio de Pádua	914,96	0,99	0,98	843,92	0,99	0,98

percentage of the area below − 0.3 standard deviations, corresponding to 3266 km^2 or 91% of its area.

In the summer period, the accumulated standard deviations were less than − 0.3 standard deviations, ranging between 271.3 and 557 mm, representing 17,145 km^2, or 40% of the RJS. In the comparison between the HRs, HR-VI (Lagos–São João) obtained the highest percentage of the classified area below − 0.3 standard deviations, corresponding to 3284 km^2, or 93% of its area.

Table 7 Classification of susceptibility to the precipitation category

Class	Z-score	Precipitation (mm)	Note	Predominant HR		
				Area (km^2)	Percentage	HR
Annual						
Very low	< − 0.3	813.6–1257	5	3266	91%	VI
Low	− 0.3–0	1258–1325	4	1199	25%	V
Average	0–1	1326–1553	3	5307	83%	III
High	1–2	1554–1780	2	646	37%	I
Very high	> 2	1781–2375	1	565	33%	I
Summer						
Very low	< − 0.3	271.3–557	5	3284	93%	VI
Low	− 0.3–0	557.1–597	4	727	17%	VIII
Average	0–1	597.1–725	3	3065	70%	VII
High	1–2	725.1–855	2	2749	78%	III
Very high	> 2	855.1–1.110	1	60	3%	I
Winter						
Very low	< − 0.3	49.1–94	5	5584	87%	III
Low	− 0.3–0	94.1–103	4	1683	12%	IX
Average	0–1	104–135	3	3449	95%	VI
High	1–2	136–167	2	2607	54%	V
Very high	> 2	168–326	1	706	41%	I

In the winter period, the accumulated standard deviations were less than − 0.3 standard deviations and ranged between 49 and 94 mm, representing 19,802 km^2, or 45% of the RJS. When comparing the HRs, HR-III (Médio Paraíba do Sul) obtained the highest percentage of the classified area below − 0.3 standard deviations, corresponding to 5584 km^2, or 87% of its area.

Temperature

The standardization of accumulated temperature in the annual, summer, and winter cycles was carried out using Eq. (1), for an average (μ) = 21.5 ℃ and standard deviation (σ) = 1.9 ℃ in the annual period; (μ) = 29.6 ℃ and (σ) = 1.8 ℃ in the summer; and (μ) = 18.8 ℃ and (σ) = 2 ℃ in winter and reclassified according to the deviation from the null value (average of observations) according to Table 8.

In the annual period, 3781 km^2, or 3% of the RJS, presented temperatures between 1 and 2 standard deviations, estimated between 23.6 and 23.8 ℃. In the comparison between the HRs, HR-II (Guandu) obtained the highest percentage of area, comprising between 1 and 2 standard deviations, corresponding to 382 km^2, or 91% of its area.

In the summer, 5286 km^2, or 12% of the RJS, showed temperatures between 1 and 2 standard deviations, estimated between 31.5 and 32.6 ℃. When comparing the HRs, HR-IX (Baixo Paraíba do Sul e Itabapoana) obtained the highest percentage of the area between 1 and 2 standard deviations, corresponding to 3887 km^2, or 29% of its area.

In winter, 4156 km^2, or 9% of the RJS, presented temperatures between 1 and 2 standard deviations, estimated between 20.4 and 21.4 ℃. In the comparison between the HRs, HR-II (Guandu) obtained the highest percentage of the area between 1 and 2 standard deviations, corresponding to 1142 km^2, or 31% of its area.

Map of susceptibility to fire risk

The susceptibility map to fire risk was created by combining and categorizing the conditions determined by the AHP method (Eq. (3)), allocating weights of normalized values between variables, and producing, on a scale of 1/5,000,000, three cartographic representations from the surface of the RJS that show the possibility of fire occurrence in the annual, winter, and summer periods.

Table 8 Classification of susceptibility to temperature

Class	Z-score	Temperature (°C)	Note	Predominant HR		
				Area (km^2)	Percentage	HR
Annual						
Very low	< − 0.3	9.5–21.0	1	4812	75%	III
Low	− 0.3–0	21.1–21.5	2	1010	16%	III
Average	0–1	21.6–23.5	3	3432	95%	VI
High	1–2	23.6–23.8	4	382	8%	II
Very high	> 2	-	5	-	-	-
Summer						
Very low	< − 0.3	16.8–29.0	1	2494	71%	IV
Low	− 0.3–0	29.0–29.6	2	1946	30%	III
Average	0–1	29.6–31.5	3	3724	77%	V
High	1–2	31.5–32.6	4	3887	29%	IX
Very high	> 2	-	5	-	-	-
Winter						
Very low	< − 0.3	7.2–18.2	1	2951	83%	IV
Low	− 0.3–0	18.2–18.8	2	975	15%	III
Average	0–1	18.8–20.8	3	3892	81%	V
High	1–2	20.8–21.4	4	1142	31%	II
Very high	> 2	-	5	-	-	-

$$\text{Susceptibility} = 0.2085P + 0.1724U + 0.1170H + 0.0897D + 0.0403O + 0.0344T + 0.0344A. \quad (3)$$

where P, U, H, D, O, T, and A are the precipitation, land use, water deficit, declivity, slope orientation, temperature, and altimetry matrices.

In the annual period, 3291 km^2, or 9% of the RJS area, was classified as having "very high" susceptibility. In this scenario, HR-IX (Baixo Paraíba do Sul e Itabapoana) was responsible for 2800 km^2 of areas highly favorable to fire foci appearance, corresponding to 7% of the total area susceptible to burning in the RJS. The accumulation of fire foci in the medium susceptibility class (Fig. 7) is notable, as this class was responsible for 47%, or 5024, fire foci between 2003 and 2017.

In summer, 84.34 km^2, or 0.2% of the RJS area, was classified as having "very high" susceptibility, which characterizes a reduction of 3817% compared to the annual period, and an accumulation of fire foci in the susceptibility class average (Fig. 7), responsible for 61%, or 400 fire foci between 2003 and 2017.

During winter, an area equivalent to 12,497 km^2, or 32% of the RJS, was classified as highly susceptible to fire foci, representing an increase of 74% in regions prone to burning events, compared to the annual period. The hydrographic regions that demonstrated extensive areas with very high susceptibilities during winter were: HR-IX, 6402 km^2, equivalent to 53% of its territory; HR-VII, with 2154 km^2, equivalent to 51% of its territory; and HR-III, with 2650 km^2, equivalent to 43% of its territory. The sum of the HR areas mentioned above represents 90% of the most critical areas in the RJS. Of interest is the accumulation of fire foci in the "high" and "very high" susceptibility classes (Fig. 6), corresponding to a total of 4852, or 68% of the fire foci, between 2003 and 2017, and 45% of the total spots in the series adopted.

Table 9 summarizes the area occupied by each susceptibility class, in square kilometers, and percentage values, indicating the dominant HR by susceptibility class. Figure 7 shows the results for the annual, summer, and winter periods.

Table 9 Classification of susceptibility in the RJS

Class	Susceptibility	Note	Area (km^2)	Percentage	HR
Annual					
Very low	0.59–1.70	1	1262.45	3%	I
Low	1.80–2.20	2	7514.27	19%	II
Average	2.30–2.50	3	15,672.06	41%	VIII
High	2.60–2.70	4	10,910.34	28%	IX
Very high	2.80–3.40	5	3291.97	9%	IX
Summer					
Very low	0.59–1.70	1	1904.89	5%	I
Low	1.80–2.20	2	8479.58	22%	II
Average	2.30–2.50	3	19,934.41	52%	VI
High	2.60–2.70	4	8212.79	21%	IX
Very high	2.80–3.40	5	84.34	0%	-
Winter					
Very low	0.59–1.70	1	780.34	2%	I
Low	1.80–2.20	2	2716.86	7%	I
Average	2.30–2.50	3	10,187.60	26%	V
High	2.60–2.70	4	12,439.08	32%	III
Very high	2.80–3.40	5	12,497.24	32%	IX

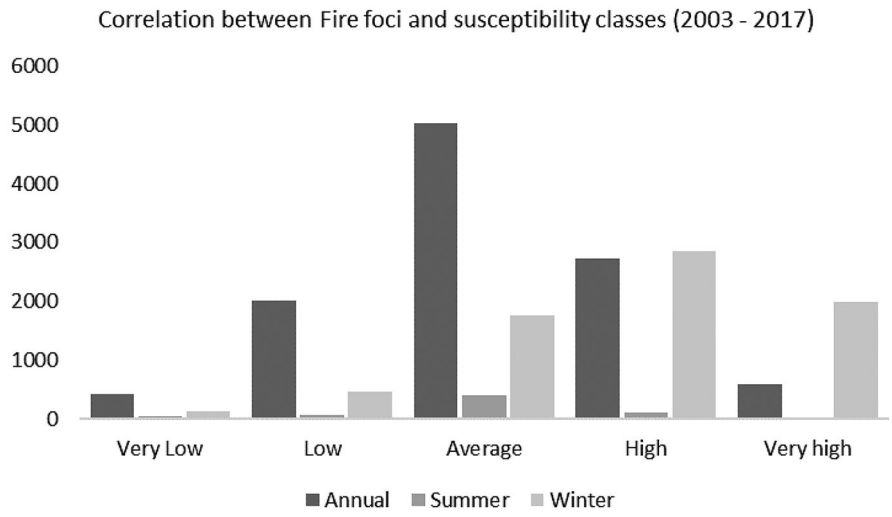

Fig. 6 Distribution of fire foci by susceptibility class in the RJS

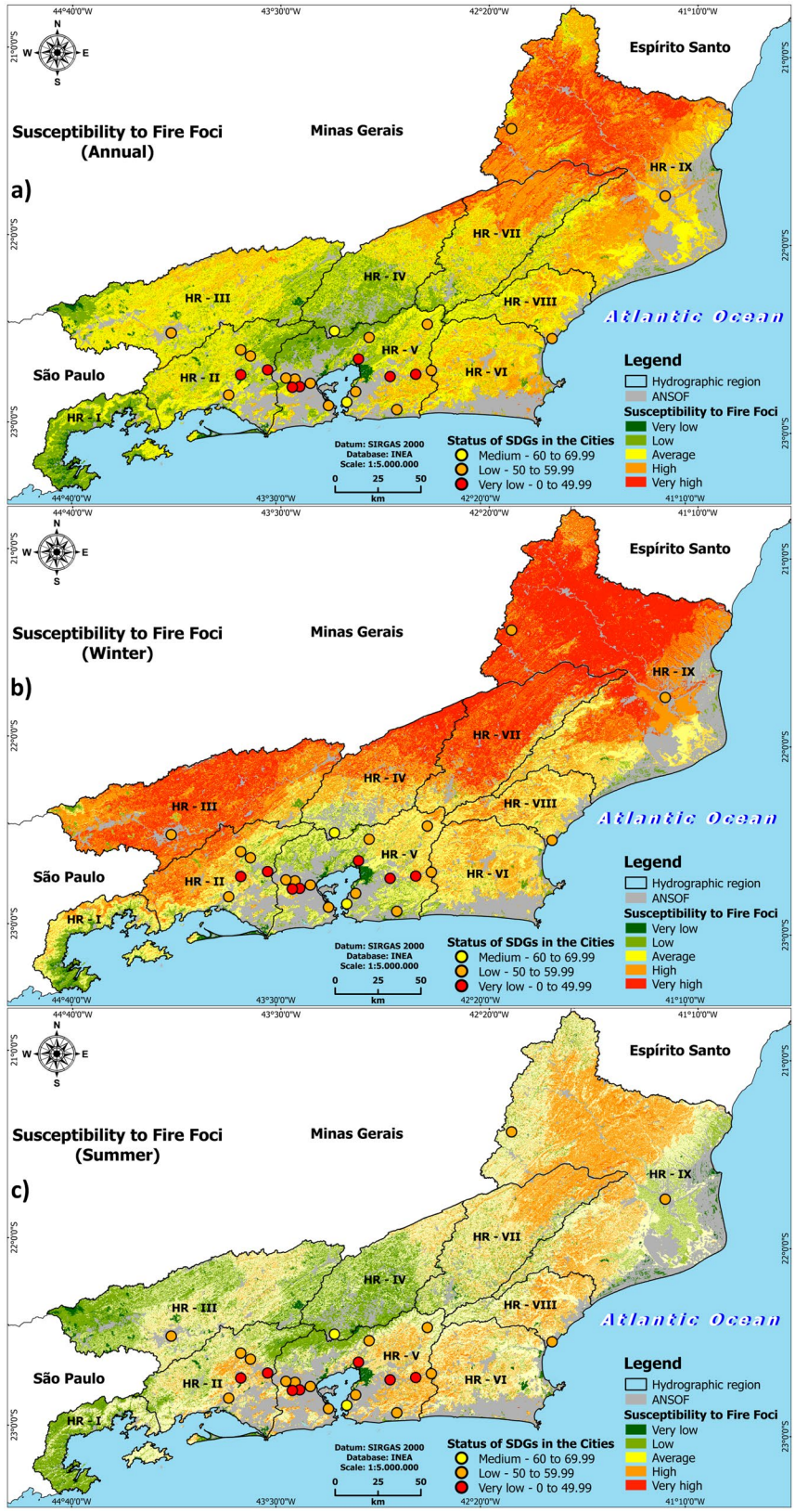

Fig. 7 Map of susceptibility to the occurrence of fire foci in the **a** annual, **b** winter, and **c** summer by hydrographic region in the RJS

Table 10 Observed values from the accumulated fire foci frequency by susceptibility class

Year	Annual					Winter					Summer				
	VL	L	A	H	VH	VL	L	A	H	VH	VL	L	A	H	VH
2003	33	164	523	256	65	12	54	176	256	192	2	1	36	9	0
2004	26	131	334	154	35	9	22	100	139	92	0	5	7	3	0
2005	26	125	286	166	19	12	32	101	142	57	1	8	17	3	0
2006	50	192	481	281	73	15	39	191	322	275	0	4	19	14	0
2007	47	311	589	261	66	16	40	202	265	229	4	5	27	6	0
2008	19	94	211	168	41	9	26	99	162	98	2	1	1	2	0
2009	14	63	157	123	23	5	12	65	101	55	2	1	10	3	0
2010	37	165	489	273	97	9	47	159	292	226	3	1	55	12	0
2011	41	193	484	262	34	8	31	149	317	171	11	4	24	12	0
2012	14	75	246	142	21	4	25	61	107	74	3	2	16	6	0
2013	15	30	175	106	23	5	18	55	105	68	6	3	3	2	0
2014	53	299	537	233	37	5	26	108	203	130	14	15	88	17	0
2015	30	83	216	130	12	7	16	56	88	42	4	11	71	17	0
2016	27	86	296	169	41	7	47	121	163	130	0	4	5	5	0
2017	27	145	419	251	41	7	32	120	191	160	4	3	21	6	0
Total	**432**	**2011**	**5024**	**2724**	**587**	**130**	**467**	**1763**	**2853**	**1999**	**56**	**68**	**400**	**117**	**0**

VL, very low; *L*, low; *A*, average; *H*, high; *VH*, very high

Relationship between fire foci and susceptibility to fire risk

From the accumulated fire foci frequency by susceptibility class, a table of observed values was built (Table 10). From the application of Eq. (2), the expected values, represented in Table 11, were established for the annual, winter, and summer periods.

The result of the statistical calculation χ^2 (Eq. 2) applied to annual and winter periods, at the 95% confidence level with 56 degrees of freedom, demonstrated the robustness of the probabilistic models

Table 11 Expected values from the application of Eq. (2)

Year	Annual					Winter					Summer				
	VL	L	A	H	VH	VL	L	A	H	VH	VL	L	A	H	VH
2003	40.98	192.47	485.91	265.58	56.06	12.44	44.68	168.67	272.96	191.25	4.19	5.09	29.95	8.76	-
2004	26.77	125.73	317.40	173.48	36.62	6.53	23.44	88.49	143.20	100.34	1.31	1.59	9.36	2.74	-
2005	24.48	115.00	290.33	158.69	33.50	6.20	22.28	84.09	136.08	95.35	2.53	3.08	18.10	5.29	-
2006	42.39	199.13	502.71	274.77	58.00	15.18	54.52	205.83	333.09	233.38	3.23	3.93	23.09	6.75	-
2007	50.15	235.55	594.66	325.03	68.61	13.56	48.69	183.83	297.48	208.44	3.67	4.46	26.21	7.67	-
2008	20.98	98.55	248.79	135.98	28.70	7.10	25.51	96.31	155.86	109.21	0.52	0.64	3.74	1.10	-
2009	14.96	70.26	177.37	96.95	20.46	4.29	15.41	58.18	94.15	65.97	1.40	1.70	9.98	2.92	-
2010	41.76	196.17	495.24	270.69	57.14	13.21	47.46	179.18	289.97	203.17	6.20	7.53	44.31	12.96	-
2011	39.91	187.48	473.30	258.70	54.61	12.19	43.77	165.25	267.42	187.37	4.46	5.41	31.83	9.31	-
2012	19.60	92.08	232.45	127.05	26.82	4.88	17.55	66.25	107.21	75.11	2.36	2.86	16.85	4.93	-
2013	13.74	64.53	162.90	89.04	18.80	4.52	16.25	61.36	99.29	69.57	1.22	1.49	8.74	2.56	-
2014	45.62	214.29	540.99	295.69	62.42	8.51	30.56	115.38	186.72	130.83	11.71	14.22	83.62	24.46	-
2015	18.54	87.08	219.85	120.16	25.37	3.77	13.53	51.09	82.68	57.93	9.00	10.93	64.27	18.80	-
2016	24.37	114.45	288.93	157.92	33.34	8.44	30.30	114.40	185.14	129.72	1.22	1.49	8.74	2.56	-
2017	34.76	163.26	412.16	225.27	47.55	9.19	33.02	124.67	201.75	141.36	2.97	3.61	21.22	6.21	-
Total	**432**	**2011**	**5024**	**2724**	**587**	**130**	**467**	**1763**	**2853**	**1999**	**56**	**68**	**400**	**117**	**0**
	X-squared = 259.73					**X-squared = 121.32**					**X-squared = 108.64**				

in evaluating the observed data set because the tabulated χ^2, equal to 79,082, was less than the χ^2_{cal}. In summer, the same event was observed statically for 42 degrees of freedom at the 95% confidence level, and the robustness of the probabilistic model to the observed data set, because the tabulated χ^2, equal to 61,656, was lower than the calculated χ^2_{cal}.

Discussion

All the results highlight that the fire foci variability in the RJS intensifies after June and peaks in September. This variability is consistent with the RJS seasons, as between June and September, the precipitation profiles are lower because of the high-pressure synoptic systems operating during winter (André et al., 2008; Brito et al., 2017; Coelho et al., 2016; Reboita et al., 2012; Sobral et al., 2020). The monthly variability in fire foci corroborates previous RJS studies (Caúla et al., 2015; Clemente et al., 2017; Nunes et al., 2015).

With regard to outliers, those of greater representativeness were identified in the years 2014 and 2015, coinciding with the prolonged drought period that affected the RJS in 2014 and 2015, when a water crisis hit the Southeast region in January 2014 and February 2015, a process that significantly favored the occurrence of forest fires and fires in several RJS regions (Otto et al., 2015; Rodrigues et al., 2018).

The prolonged drought that occurred in January 2014 and February 2015, on the other hand, favored the appearance of fire foci in the summer period, regions that are typically classified as low and very low.

During each analyzed year, the quarter with the highest occurrence of fire foci corresponds to the transition period between winter and spring. These seasons are typically distinguished by the occurrence of dry spells, long dry periods, low air humidity, and a dry air mass in the Southeast region (Brito et al., 2017; Grimm, 2003; Reboita et al., 2010). The rainy season in the southeast region begins in October in normal years (Minuzzi et al., 2007), which may explain the high number of fire foci in the months preceding the rainy season, particularly in the RJS.

The Climatic Analysis Bulletin (INPE, 2014) reported that an atmospheric blockage (AB) inhibited the formation of the South Atlantic convergence zone (SACZ), changing the rain regime quality. In 2015, due to the formation of an intense high-level cyclonic vortex (HLCV) of 250 hPA over NEB, the precipitation patterns in the southeast were affected by negative precipitation anomalies, a factor associated with the strong stability of the system synoptic, inhibiting cloud formation and storm cloud development. Simultaneously, it blocked the entry of frontal systems (FS) from the southern portion of South America, which is a fundamental mechanism in total regional precipitation production during the southern summer, and favored environmental humidity reduction, increasing fire propagation potential, and hindering the actions aimed at its control, a situation that explains the increase of fire foci in 2014 and 2015 (Braga & Molion, 2018; Sausen & Lacruz, 2015).

Changes in soil use and cover, such as new agricultural boundaries and urban-forestry expansion processes, make exposed areas more vulnerable to burns and fires (Badia et al., 2019; Cardil et al., 2020). However, according to the adopted mapping of land use and land cover (INEA, 2021), between the years 2010 and 2015, no amendments compatible with the scale used were detected in ANSOF areas, resulting in changes in the identification of regions not prone to the emergence of fire focis in RJS. In this regard, possible changes in areas of ANSOF that impact the identification of regions susceptible to fire focis necessitate a cartographic scale with additional detail.

HRs I and IV showed the greatest declivity in the RJS, which facilitated the spread of fire foci (Adab et al., 2013; Prudente & Rosa, 2010; Torres et al., 2014). Their access and extinction was made difficult (Badia-Perpinyà & Pallares-Barbera, 2006) as they were mainly in environmental protection areas (Camargo et al., 2019; Coura et al., 2011; Fernandes et al., 2011) and the forest fire sites had high extension and duration, resulting in the loss of the original fauna and flora (Aximoff, 2011; Rodrigues et al., 2018), intensifying the ongoing forest fragmentation, and promoting an increase in the vulnerability and ecological instability of forest remnants (Lima et al., 2017). The HR-III (Médio Paraíba do Sul), HR-VII (Rio Dois Rios), and HR-IX (Baixo Paraíba do Sul e Itabapoana) were identified in more than 50% of areas composed of fields/pastures, a use that favors fire appearance, especially in dry periods, with a strong presence of sugarcane cultivation in HR-IX. Factors that favor fire foci emergence are

directly associated with the adoption of the practice of burning sugarcane fields in the pre-harvest season, a typical action in Brazil, driven by economic, environmental, and cultural factors, especially in Rio de Janeiro and São Paulo states (França et al., 2014). Consistent with these factors, the aforementioned HRs have the highest evapotranspiration rates (Araújo et al., 2007; Fernandes et al., 2011), as well as the highest temperatures and the lowest accumulated precipitation (INEA, 2011), consequences that are reflected in the loss of moisture from plant biomass (Sausen & Lacruz, 2015), and favor the appearance of fire foci. In this sense, in the annual period, as it presents 2800 km^2 of areas subject to the appearance of fire foci, HR-IX is distinguished from the other hydrographic regions of the RJS because of the high level of susceptibility and numerous records of fire foci in the region.

In the summer, mainly in SEB (Barcellos & Quadro, 2019; Coelho & Nunes, 2020), the main rainmakers in the RJS are the SACZ (Coelho & Nunes, 2020), frontal systems (Dereczynski et al., 2009; Seluchi & Chou, 2009; Seluchi et al., 2016), isolated convective systems (Silva & Dereczynski, 2014), or even the association among these systems (Moura et al., 2013), which can cause significant variations in the spatial organization and precipitation intensity, modifying the moisture content of the combustible material available on the surface (Sausen & Lacruz, 2015), making it difficult, or even impossible, for the appearance and propagation of fire foci. When compared to the regional climatological pattern, the prolonged drought that occurred in January 2014 and February 2015 favored the appearance of fire focis in the summer period, regions typically classified in the low and very low range.

During winter, the reduction in precipitation accumulations (Silva & Dereczynski, 2014; Sobral et al., 2018) and the increase in evapotranspiration rates (Anjos et al., 2016), which characterize the RJS dry season, justify the increase in areas classified as high and very high susceptibility in the following hydrographic regions: HR-IX (Baixo Paraíba do Sul e Itabapoana), HR-VII (Rio Dois Rios), HR-IV (Piabanha), HR-III (Médio Paraíba do Sul), HR- II (Guandu), HR-IV (Piabanha), and HR-V (Baía de Guanabara). Regions that integrate several important areas of environmental protection in the RJS, especially in the mountainous and southern regions of the state, where the following stand out: Petrópolis Environmental Protection Area, Serra dos Órgãos National Park (PARNASO), Araras Biological Reserve, Itatiaia National Park, and similar areas. These areas are classified as having high and very high susceptibility levels during winter, a result that converges with the records found by (Aximoff & Rodrigues, 2011; Nunes et al., 2015; Rodrigues et al., 2018).

In the SDGs context, the majority of municipalities in the RJS are located in HR-II (Guandu) and HR-V (Baía de Guanabara), areas with average susceptibility to fire in the annual, winter, and summer periods, with a similar situation in HR-VI (Piabanha) and HR-VIII (Macaé and Ostras). Municipalities in HR-III (Médio Paraíba do Sul) and HR-IX (Baixo Paraíba do Sul e Itabapoana) have medium-to-high susceptibility in the annual and summer periods and high to very high in the winter, drier period, characterizing the regions with the highest vulnerability to the occurrence of fires, primarily in Volta Redonda (HR-III) and Miracema (HR-IX).

The intersection between the registered fire foci and the pixels classified into different susceptibility classes, using the χ^2 statistic, demonstrated a dependent relationship among the listed variables, indicating that the predictive models adhere to the events in loco. In this regard, the hypothesis of increased vulnerability to the emergence of burnings in HR-II, III, IV, V, VII, and IX during the winter period is congruent with the statistical test used because, in winter, 68% of the fire focis focused on pixels classified between high and very high classes, with a high concentration of fire focis in the aforementioned regions, similar to the results obtained by Clemente et al. (2017), which highlighted the increase in the concentration of fire focis. HR-VII and IX concentrated areas of greater susceptibility to fire focis over the annual period, with HR-IX presenting regions of moderate susceptibility to desertification (Bohn et al., 2021; Santos et al., 2022), as well as low pluviometric indices, high temperatures, and high evapotranspiration rates. During the summer, areas of greater vulnerability to fire focis are concentrated in the RJS's coastal regions, and areas of high susceptibility are not detected. The results show that the spatial–temporal variation of fire focis can influence the standard of vegetable cover (Andrade et al., 2019; Freitas et al., 2020; Silva, 2019) because environmental factors and forest structure have a large influence on fire initiation (Sivrikaya & Küçük, 2022), due to the geographical extent of the areas indicated with high and very high susceptibility.

In this context, digital technologies used for the establishment of vulnerable areas to burn in periods are relevant in the context of the application of SGDs (Pigola et al., 2021) because such tools favor analyses on burn prevention (Abedi Gheshlaghi et al., 2021), reduction of emissions from atmospheric pollutants, as well as impacts on the most vulnerable populations (Afrin & Garcia-Menendez, 2021; Marlier et al., 2020), and the sustainable management of economic and environmental resources. Such factors contribute to the efforts and challenges of achieving sustainability in the 92 municipalities of RJS in their social, economic, institutional, and environmental dimensions, thereby reducing pressure on natural resources and the negative impacts that result.

Conclusions

The results should support spatial analysis and decision-making on the subject, with the potential to subsidize, allow, and facilitate the assessment, analysis, and management of these phenomena on local and regional scales, as well as their planning and control by public institutions.

According to the RJS's temporal evaluation of fires, the most critical is June, with a peak in September and a fall from November onwards. In the winter, there is an increase in the absolute number of records of fire focis associated with a decrease in precipitation and an increase in the number of HRs with high susceptibility to fire in the RJS, primarily compromising environmental preservation areas.

The chi-square statistics confirmed the association between fire focis and the susceptibility of areas classified as "very low" to "very high," confirming the effectiveness of factors that exacerbate the emergence of fire focis and the hierarchical analysis method used, resulting in a method that can be replicated in other states in Brazil and around the world.

In the SDGs context, the majority of the municipalities covered by the RJS are located in areas with a year-round susceptibility to fire. Regions with high-to-very high susceptibility are critical during the driest period (winter), which may impede future SDG adoption for municipalities located in these areas, particularly Volta Redonda (HR-III) and Miracema (HR-IX).

The mapping of fire foci, which includes data, information, and the identification of areas most vulnerable to forest fires, can assist institutions and response agencies (environmental agency, civil defense, and health system) in the implementation of contingency plans and combat protocols for forest fires. The susceptibility results support a variety of actions for the environmental agency and civil defense, including promoting management for fire suppression, particularly during critical periods and drought, and for the health system, specifically noting the drop in air quality standards and an increase in hospital admissions. Such consequences necessitate the adoption of structural and non-structural measures by the government, whose resources destined for prevention, response, and recovery are better used when the areas of greatest criticality and vulnerability are identified.

Acknowledgements We would like to thank the reviewers for their consideration and contributions, the Military Fire Brigade of Rio de Janeiro State (CBMERJ), and the State Center for Natural Disasters Monitoring and Alerting (CEMADEN—RJ). The Graduate Program in Meteorology (PPGM/UFRJ) and the Civil Engineering Program (PEC/COPPE/UFRJ) supported the development of this research.

Declarations

Conflict of interests The authors declare no competing interests.

References

Abedi Gheshlaghi, H., Feizizadeh, B., Blaschke, T., Lakes, T., & Tajbar, S. (2021). Forest fire susceptibility modeling using hybrid approaches. *Transactions in GIS, 25*(1), 311–333. https://doi.org/10.1111/tgis.12688

Abedi Gheshlaghi, H. A. (2019). Using GIS to develop a model for forest fire risk mapping. *Journal of the Indian Society of Remote Sensing, 47*(7), 1173–1185. https://doi.org/10.1007/s12524-019-00981-z

Adab, H., Kanniah, K. D., & Solaimani, K. (2021). Remote sensing-based operational modeling of fuel ignitability in Hyrcanian mixed forest, Iran. *Natural Hazards, 108*(1), 253–283. https://doi.org/10.1007/s11069-021-04678-w

Adab, H., Kanniah, K. D., & Solaimani, K. (2013). Modeling forest fire risk in the northeast of Iran using remote sensing and GIS techniques. *Natural Hazards, 65*(3), 1723–1743. https://doi.org/10.1007/s11069-012-0450-8

Afrin, S., & Garcia-Menendez, F. (2021). Potential impacts of prescribed fire smoke on public health and socially

vulnerable populations in a Southeastern US state. *Science of the Total Environment, 794*, 148712. https://doi.org/10.1016/j.scitotenv.2021.148712

Ager, A. A., Evers, C. R., Day, M. A., Alcasena, F. J., & Houtman, R. (2021). Planning for future fire: Scenario analysis of an accelerated fuel reduction plan for the western United States. *Landscape and Urban Planning, 215*, 104212. https://doi.org/10.1016/j.landurbplan.2021.104212

Altay, N., Prasad, S., & Tata, J. (2013). A dynamic model for costing disaster mitigation policies. *Disasters, 37*(3), 357–373. https://doi.org/10.1111/disa.12004

Alvares, C. A., Stape, J. L., Sentelhas, P. C., & de Moraes Gonçalves, J. L. (2013). Modeling monthly mean air temperature for Brazil. *Theoretical and Applied Climatology, 113*(3), 407–427. https://doi.org/10.1007/s00704-012-0796-6

Andrade, C. F., Duarte, J. B., Barbosa, M. L. F., de Andrade, M. D., de Oliveira, R. O., Delgado, R. C., Pereira, M. G., Batista, T. S., & Teodoro, P. E. (2019). Fire outbreaks in extreme climate years in the State of Rio de Janeiro, Brazil. *Land Degradation & Development, 30*(11), 1379–1389. https://doi.org/10.1002/ldr.3327

André, R. G. B., Marques, V. D. S., Pinheiro, F. M. A., & Ferraudo, A. S. (2008). Identificação de regiões pluviometricamente homogêneas no estado do Rio de Janeiro, utilizando-se valores mensais. *Revista Brasileira De Meteorologia, 23*, 501–509. https://doi.org/10.1590/S0102-77862008000400009

Anjos, A. W. dos, Delgado, R. C., Lyra, G. B., de Souza, L. P., & Suhett, E. R. (2016). Evapotranspiração a partir de produtos orbitais para o estado do Rio de Janeiro. *Irriga, 1*(01), 126–126. https://doi.org/10.15809/irriga.2016v1n01p126-140

Aragão, L. E. O., Malhi, Y., Roman-Cuesta, R. M., Saatchi, S., Anderson, L. O., & Shimabukuro, Y. E. (2007). Spatial patterns and fire response of recent Amazonian droughts. *Geophysical Research Letters, 34*(7), 1–5. https://doi.org/10.1029/2006GL028946

Araújo, W. F., Costa, S. A. A., & dos Santos, A. E. (2007). Comparação entre métodos de estimativa da evapotranspiração de referência (ETo) para Boa Vista, RR. *Revista Caatinga, 20*(4), 84–88.

Aximoff, I. (2011). O que Perdemos com a Passagem do Fogo pelos Campos de Altitude do Estado do Rio de Janeiro?. *Biodiversidade Brasileira-BioBrasil*, *2*, 180–200. https://doi.org/10.37002/biobrasil.v%25vi%25i.139

Aximoff, I., & Rodrigues, R. D. C. (2011). Histórico dos incêndios florestais no Parque Nacional do Itatiaia. *Ciência Florestal, 21*(1), 83–92. https://doi.org/10.5902/198050982750

Aximoff, I. A., Fraga, C. N., & Bovini, M. G. (2016). Vegetação em afloramentos rochosos litorâneos perturbados por incêndios na Região Metropolitana Fluminense, estado do Rio de Janeiro. *Biodiversidade Brasileira-BioBrasil*, *2*, 149–172. https://doi.org/10.37002/biobrasil.v%25vi%25i.536

Badia, A., Pallares-Barbera, M., Valldeperas, N., & Gisbert, M. (2019). Wildfires in the wildland-urban interface in Catalonia: Vulnerability analysis based on land use and land cover change. *Science of the Total Environment, 673*, 184–196. https://doi.org/10.1016/j.scitotenv.2019.04.012

Badia-Perpinyà, A., & Pallares-Barbera, M. (2006). Spatial distribution of ignitions in Mediterranean periurban and rural areas: The case of Catalonia. *International Journal of Wildland Fire, 15*(2), 187–196. https://doi.org/10.1071/WF04008

Barcellos, D. R., & de Quadro, M. F. L. (2019). Classificação de eventos extremos de precipitação quanto sua intensidade, persistência e abrangência na região das ZCAS. *Metodologias e Aprendizado, 2*, 76–81. https://doi.org/10.21166/metapre.v2i0.1320

Behling, H., Jantz, N., & Safford, H. D. (2020). Mid-and late Holocene vegetation, climate and fire dynamics in the Serra do Itatiaia, Rio de Janeiro State, southeastern Brazil. *Review of Palaeobotany and Palynology, 274*, 104152. https://doi.org/10.1016/j.revpalbo.2019.104152

Bergonse, R., Oliveira, S., Gonçalves, A., Nunes, S., DaCamara, C., & Zêzere, J. L. (2021). Predicting burnt areas during the summer season in Portugal by combining wildfire susceptibility and spring meteorological conditions. *Geomatics, Natural Hazards and Risk, 12*(1), 1039–1057. https://doi.org/10.1080/19475705.2021.1909664

Bohn, L., Lyra, G. B., Oliveira-Júnior, J. F., Zeri, M., & Cunha-Zeri, G. (2021). Desertification susceptibility over Rio de Janeiro, Brazil, based on aridity indices and geoprocessing. *International Journal of Climatology, 41*, E2600–E2614. https://doi.org/10.1002/joc.6869

Bowman, D. M., Kolden, C. A., Abatzoglou, J. T., Johnston, F. H., van der Werf, G. R., & Flannigan, M. (2020). Vegetation fires in the Anthropocene. *Nature Reviews Earth & Environment, 1*(10), 500–515. https://doi.org/10.1038/s43017-020-0085-3

Braga, H. A., & Molion, L. C. B. (2018). A Seca de 2013/2014 na Região Sudeste do Brasil. *Anuário do Instituto de Geociências, 41*(1), 100–107. https://doi.org/10.11137/2018_1_100_107

Brito, T. T., Oliveira-Júnior, J. F., Lyra, G. B., Gois, G., & Zeri, M. (2017). Multivariate analysis applied to monthly rainfall over Rio de Janeiro state, Brazil. *Meteorology and Atmospheric Physics, 129*(5), 469–478. https://doi.org/10.1007/s00703-016-0481-x

de Souza Camargo, L., da Silva, R. W., do Amaral, S. S., da Silva, A. P., Ferreli, T., & da Silva, M. P. D. (2019). Mapeamento de Áreas Susceptíveis a Incêndios Florestais do Município de Petrópolis–RJ. *Anuário do Instituto de Geociências, 42*(1), 630–641. https://doi.org/10.11137/2019_1_630_641

Cardil, A., De-Miguel, S., Silva, C. A., Reich, P. B., Calkin, D., Brancalion, P. H., Vibrans, A. C., Gamarra, J. G. P., Zhou, M., Pijanowski, B. C., Hui, C., Crowther, T. W., Hérault, B., Piotto, D., Salas-Eljatib, C., Broadbent, E. N., Zambrano, A. M. A., Picard, N., Aragão, L. E. O. C., Liang, J. (2020). Recent deforestation drove the spike in Amazonian fires. *Environmental Research Letters, 15*(12), 121003. https://doi.org/10.1088/1748-9326/abcac7

Cardil, A., & Molina, D. M. (2015). Factors causing victims of wildland fires in Spain (1980–2010). *Human and Ecological Risk Assessment: An International Journal, 21*(1), 67–80. https://doi.org/10.1080/10807039.2013.871995

Castro, J. D. S., Costa, L. S., Barbosa, G. R., Assemany, P. P., & Calijuri, M. L. (2015). Utilização de SIG e análise multicritério para seleção de áreas com potencial para a construção de universidades e loteamentos universitários. *Boletim De Ciências Geodésicas, 21*, 652–657. https://doi.org/10.1590/S1982-21702015000300037

Caúla, R. H., Oliveira-Júnior, J. F., Lyra, G. B., Delgado, R. C., & Heilbron Filho, P. F. L. (2015). Overview of fire foci causes and locations in Brazil based on meteorological satellite data from 1998 to 2011. *Environmental Earth Sciences, 74*(2), 1497–1508. https://doi.org/10.1007/s12665-015-4142-z

Cerdà, A. (2020). The Role of fire in achieving the sustainable development goals of the United Nations. *Multidisciplinary Digital Publishing Institute Proceedings, 30*(1), 65. https://doi.org/10.3390/proceedings2019030065

Chandler, S. E. (1982). The effects of severe weather conditions on the incidence of fires in dwellings. *Fire Safety Journal, 5*(1), 21–27. https://doi.org/10.1016/0379-7112(82)90004-2

Charre, J. (1995). *Statistique et territoire*. Gip Reclus. ISBN2–86912–060–2.

Chuvieco, E., & Congalton, R. G. (1989). Application of remote sensing and geographic information systems to forest fire hazard mapping. *Remote Sensing of Environment, 29*(2), 147–159. https://doi.org/10.1016/0034-4257(89)90023-0

Clemente, S. D. S., Oliveira, J. F. D., & Passos Louzada, M. A. (2017). Focos de calor na Mata Atlântica do Estado do Rio de Janeiro. *Revista Brasileira De Meteorologia, 32*, 669–677. https://doi.org/10.1590/0102-7786324014

Coelho, C. A., de Oliveira, C. P., Ambrizzi, T., Reboita, M. S., Carpenedo, C. B., Campos, J. L. P. S., Tomaziello, A. C. N., Pampuch, L. A., Custódio, M. S., Dutra, L. M. M., da Rocha, R. P., & Rehbein, A. (2016). The 2014 southeast Brazil austral summer drought: Regional scale mechanisms and teleconnections. *Climate Dynamics, 46*(11), 3737–3752. https://doi.org/10.1007/s00382-015-2800-1

Coelho, L. A. F., & Nunes, A. B. (2020). Eventos Recentes de Chuva Intensa na Cidade do Rio de Janeiro: Análise Sinótica. *Revista Brasileira de Geografia Física, 13*(03), 994–1012. https://doi.org/10.26848/rbgf.v13.3.p994-1012

Corcoran, J., Higgs, G., Rohde, D., & Chhetri, P. (2011). Investigating the association between weather conditions, calendar events and socio-economic patterns with trends in fire incidence: An Australian case study. *Journal of Geographical Systems, 13*(2), 193–226. https://doi.org/10.1007/s10109-009-0102-z

Coura, P. H. F., de Sousa, G. M., do Couto Fernandes, M., & de Souza Avelar, A. (2011). O uso de variáveis geomorfológicas no estudo da suscetibilidade à ocorrência de incêndios no estado do Rio de Janeiro. *Revista de Geografia (Recife), 27*(2. Esp), 210–221.

Cronemberger, F. M., Vicens, R. S., Bastos, J. S., Fevrier, P. V. R., & Barroso, G. M. (2011). Mapeamento Bioclimático do estado do Rio de Janeiro. *INPE, Anais XV Simpósio Brasileiro de Sensoriamento Remoto, Curitiba, Paraná,* 5745–5752.

Davis, E. G., & Naghettini, M. C. (2000). *Estudo de chuvas intensas no estado do Rio de Janeiro* (2nd ed.). Companhia de Pesquisa de Recursos Minerais – CPRM.

Dereczynski, C. P., Oliveira, J. S. D., & Machado, C. O. (2009). Climatologia da precipitação no município do Rio de Janeiro. *Revista Brasileira De Meteorologia, 24*(1), 24–38. https://doi.org/10.1590/S0102-77862009000100003

de Oliveira, G., Chen, J. M., Mataveli, G. A., Chaves, M. E., Seixas, H. T., Cardozo, F. D. S., Shimabukuro, Y. E., He, L., Stark, S. C., & dos Santos, C. A. (2020). Rapid recent deforestation incursion in a vulnerable indigenous land in the Brazilian Amazon and fire-driven emissions of fine particulate aerosol pollutants. *Forests, 11*(8), 829. https://doi.org/10.3390/f11080829

Dickman, C. R. (2021). Ecological consequences of Australia's "Black Summer" bushfires: Managing for recovery. *Integrated Environmental Assessment and Management, 17*(6), 1162–1167. https://doi.org/10.1002/ieam.4496

dos Santos, J. C., Lyra, G. B., Abreu, M. C., de Oliveira-Júnior, J. F., Bohn, L., Cunha-Zeri, G., & Zeri, M. (2022). Aridity indices to assess desertification susceptibility: A methodological approach using gridded climate data and cartographic modeling. *Natural Hazards, 111*, 2531–2558. https://doi.org/10.1007/s11069-021-05147-0

dos Santos, A. M., da Silva, C. F. A., Rudke, A. P., & de Oliveira Soares, D. (2021). Dynamics of active fire data and their relationship with fires in the areas of regularized indigenous lands in the Southern Amazon. *Remote Sensing Applications: Society and Environment, 23*, 100570. https://doi.org/10.1016/j.rsase.2021.100570

Eslami, R., Azarnoush, M., Kialashki, A., & Kazemzadeh, F. (2021). GIS-based forest fire susceptibility assessment by random forest, artificial neural network and logistic regression methods. *Journal of Tropical Forest Science, 33*(2), 173–184. https://doi.org/10.26525/jtfs2021.33.2.173

Fávero, L. P., & Belfiore, P. (2017). *Manual de Análise de Dados: Estatística e Modelagem Multivariada com Excel®, SPSS® e Stata®*. Elsevier Brasil.

Fernandes, M. D. C., Coura, P. H. F., Sousa, G. M. D., & Avelar, A. D. S. (2011). Avaliação geoecológica de susceptibilidade à ocorrência de incêndios no estado do Rio de Janeiro, Brasil. *Floresta e Ambiente, 18*(3), 299–309. https://doi.org/10.4322/floram.2011.050

Ferraz, S. F., & Vettorazzi, C. A. (1998). Mapeamento de risco de incêndios florestais por meio de sistema de informações geográficas (SIG). *Scientia Forestalis, Piracicaba, 53*, 39–48. https://doi.org/10.1590/2179-8087.025615

Ferreira, M. C. (2017). *Iniciação à análise geoespacial: Teoria, técnicas e exemplos para geoprocessamento* (1st ed.). UNESP Digital.

Fick, S. E., & Hijmans, R. J. (2017). WorldClim 2: New 1-km spatial resolution climate surfaces for global land areas. *International Journal of Climatology, 37*(12), 4302–4315. https://doi.org/10.1002/joc.5086

FIDERJ - Fundação Instituto de Desenvolvimento Econômico e Social do Rio de Janeiro. (1978). *Indicadores Climatológicos do Estado do Rio de Janeiro*. Fundação Instituto de Desenvolvimento Econômico e Social do Rio de Janeiro. Accessed 25 Apr 2021, https://biblioteca.ibge.gov.br/biblioteca-catalogo.html?id=217801&view=detalhes

França, D., Longo, K., Rudorff, B., Aguiar, D., Freitas, S., Stockler, R., & Pereira, G. (2014). Pre-harvest sugarcane burning emission inventories based on remote sensing data in the state of São Paulo, Brazil. *Atmospheric Environment, 99*, 446–456. https://doi.org/10.1016/j.atmosenv.2014.10.010

Freitas, W. K., Gois, G., Pereira, E. R., Jr., Junior, J. O., Magalhães, L. M. S., Brasil, F. C., & Sobral, B. S. (2020).

Influence of fire foci on forest cover in the Atlantic Forest in Rio de Janeiro, Brazil. *Ecological Indicators, 115*, 106340. https://doi.org/10.1016/j.ecolind.2020.106340

Ganteaume, A., Camia, A., Jappiot, M., San-Miguel-Ayanz, J., Long-Fournel, M., & Lampin, C. (2013). A review of the main driving factors of forest fire ignition over Europe. *Environmental Management, 51*(3), 651–662. https://doi.org/10.1007/s00267-012-9961-z

Ghorbanzadeh, O., Rostamzadeh, H., Blaschke, T., Gholaminia, K., & Aryal, J. (2018). A new GIS-based data mining technique using an adaptive neuro-fuzzy inference system (ANFIS) and k-fold cross-validation approach for land subsidence susceptibility mapping. *Natural Hazards, 94*(2), 497–517. https://doi.org/10.1007/s11069-018-3449-y

Gois, G. D., Freitas, W. K. D., & Oliveira Júnior, J. F. D. (2020). Spatial-temporal of fire foci in the state of Rio de Janeiro, Brazil. *Bioscience journal (Online), 36*(3): 1008–1017. https://doi.org/10.14393/BJ-v36n3a2020-47769

Grimm, A. M. (2003). The El Niño impact on the summer monsoon in Brazil: Regional processes versus remote influences. *Journal of Climate, 16*(2), 263–280. https://doi.org/10.1175/1520-0442(2003)016%3c0263:TENIOT%3e2.0.CO;2

Haines, A., Amann, M., Borgford-Parnell, N., Leonard, S., Kuylenstierna, J., & Shindell, D. (2017). Short-lived climate pollutant mitigation and the Sustainable Development Goals. *Nature Climate Change, 7*(12), 863–869. https://doi.org/10.1038/s41558-017-0012-x

Hill, J., Von Maltitz, G., Sommer, S., Reynolds, J., Hutchinson, C., & Cherlet, M. (2018). *World Atlas of desertification: Rethinking land degradation and sustainable land management*. Joint Research Centre, Publications Office.

IBGE - Instituto Brasileiro de Geografia e Estatistica. (2021). *IBGE Cidades@*. Instituto Brasileiro de Geografia e Estatistica. Accessed 3 Aug 2021, from https://cidades.ibge.gov.br/brasil/rj/panorama

INEA - Instituto Estadual do Ambiente. (2021). *GeoINEA: Base de Dados Geoespaciais*. Instituto Estadual do Ambiente. Accessed 3 Aug 2021, from https://inea.maps.arcgis.com/apps/MapSeries/index.html?appid=00cc256c620a4393b3d04d2c34acd9ed

INEA - Instituto Estadual do Ambiente. (2011). *O Estado do Ambiente: Indicadores do Rio de Janeiro 2010*. Instituto Estadual do Ambiente. Accessed 3 Aug 2021, from http://www.inea.rj.gov.br/wp-content/uploads/2019/01/Livro_O-Estado-do-Ambiente.pdf

INMET - Instituto Nacional de Meteorologia. (2022). *Normais Climatológicas do Brasil*. Instituto Nacional de Meteorologia. Accessed 25 Apr 2021, from https://portal.inmet.gov.br/normais

INPE - Instituto Nacional de Pesquisas Espaciais. (2022). *AQUA – Aqua Project Science*. Instituto Nacional de Pesquisas Espaciais. Accessed 25 Apr 2021, from http://www.dgi.inpe.br/documentacao/satelites/aqua

INPE - Instituto Nacional de Pesquisas Espaciais. (2021). *BDQueimadas - Programa Queimadas - INPE*. Instituto Nacional de Pesquisas Espaciais. Accessed 3 Aug 2021, from https://queimadas.dgi.inpe.br/queimadas/bdqueimadas

INPE - Instituto Nacional de Pesquisas Espaciais. (2014). *Climanálise - Boletim*. Instituto Nacional de Pesquisas Espaciais. Accessed 3 Aug 2021, from http://climanalise.cptec.inpe.br/~rclimanl/boletim/index0114.shtml

Justice, C., Giglio, L., Boschetti, L., Roy, D., Csiszar, I., Morisette, J., & Kaufman, Y. (2006). *Algorithm technical background document MODIS fire products*. MODIS Science Team. Accessed 3 Aug 2021, ftp://ladsweb.nascom.nasa.gov

Kiely, L., Spracklen, D. V., Arnold, S. R., Papargyropoulou, E., Conibear, L., Wiedinmyer, C., Note, C., & Adrianto, H. A. (2021). Assessing costs of Indonesian fires and the benefits of restoring peatland. *Nature Communications, 12*(1), 1–11. https://doi.org/10.1038/s41467-021-27353-x

Kodama, Y. M. (1993). Large-scale common features of subtropical convergence zones (the Baiu Frontal Zone, the SPCZ, and the SACZ) Part II: Conditions of the circulations for generating the STCZs. *Journal of the Meteorological Society of Japan. Ser. II, 71*(5), 581–610. https://doi.org/10.2151/jmsj1965.70.4_813

Kodama, Y. M. (1992). Large-scale common features of subtropical precipitation zones (the Baiu frontal zone, the SPCZ, and the SACZ) Part I: Characteristics of subtropical frontal zones. *Journal of the Meteorological Society of Japan. Ser. II, 70*(4), 813–836. https://doi.org/10.2151/jmsj1965.70.4_813

Kolden, C. A., & Abatzoglou, J. T. (2018). Spatial distribution of wildfires ignited under katabatic versus non-katabatic winds in Mediterranean Southern California USA. *Fire, 1*(2), 19. https://doi.org/10.3390/fire1020019

Kousky, V. E. (1988). Pentad outgoing longwave radiation climatology for the South American sector. *Revista Brasileira De Meteorologia, 3*(1), 217–231.

Kumari, B., & Pandey, A. C. (2020). Geo-informatics based multi-criteria decision analysis (MCDA) through analytic hierarchy process (AHP) for forest fire risk mapping in Palamau Tiger Reserve, Jharkhand state, India. *Journal of Earth System Science, 129*(1), 1–16. https://doi.org/10.1007/s12040-020-01461-6

Lautenberger, C. (2017). Mapping areas at elevated risk of large-scale structure loss using Monte Carlo simulation and wildland fire modeling. *Fire Safety Journal, 91*, 768–775. https://doi.org/10.1016/j.firesaf.2017.04.014

Leuenberger, M., Parente, J., Tonini, M., Pereira, M. G., & Kanevski, M. (2018). Wildfire susceptibility mapping: Deterministic vs. stochastic approaches. *Environmental Modelling & Software, 101*, 194–203. https://doi.org/10.1016/j.envsoft.2017.12.019

Lima, A. O., Lyra, G. B., Abreu, M. C., Oliveira-Júnior, J. F., Zeri, M., & Cunha-Zeri, G. (2021). Extreme rainfall events over Rio de Janeiro State, Brazil: Characterization using probability distribution functions and clustering analysis. *Atmospheric Research, 247*, 105221. https://doi.org/10.1016/j.atmosres.2020.105221

Lima, B. C., Francisco, C. N., & Bohrer, C. B. D. A. (2017). Deslizamentos e fragmentação florestal na região serrana do Estado do Rio de Janeiro. *Ciência Florestal, 27*, 1283–1295. https://doi.org/10.5902/1980509830321

Littell, J. S., Peterson, D. L., Riley, K. L., Liu, Y., & Luce, C. H. (2016). A review of the relationships between drought and forest fire in the United States. *Global Change Biology, 22*(7), 2353–2369. https://doi.org/10.1111/gcb.13275

Lorentz, J. F., Calijuri, M. L., Marques, E. G., & Baptista, A. C. (2016). Multicriteria analysis applied to landslide

susceptibility mapping. *Natural Hazards, 83*(1), 41–52. https://doi.org/10.1007/s11069-016-2300-6

Lowe, J. A., & Bernie, D. (2018). The impact of Earth system feedbacks on carbon budgets and climate response. *Philosophical Transactions of the Royal Society a: Mathematical, Physical and Engineering Sciences, 376*(2119), 20170263. https://doi.org/10.1098/rsta.2017.0263

Lyra, G. B., Correia, T. P., de Oliveira-Júnior, J. F., & Zeri, M. (2018). Evaluation of methods of spatial interpolation for monthly rainfall data over the state of Rio de Janeiro, Brazil. *Theoretical and Applied Climatology, 134*(3), 955–965. https://doi.org/10.1007/s00704-017-2322-3

Majdi, M., Turquety, S., Sartelet, K., Legorgeu, C., Menut, L., & Kim, Y. (2019). Impact of wildfires on particulate matter in the Euro-Mediterranean in 2007: Sensitivity to some parameterizations of emissions in air quality models. *Atmospheric Chemistry and Physics, 19*(2), 785–812. https://doi.org/10.5194/acp-19-785-2019

Marlier, M. E., Bonilla, E. X., & Mickley, L. J. (2020). How do Brazilian fires affect air pollution and public health?. *GeoHealth, 4*(12), e2020GH000331. https://doi.org/10.1029/2020GH000331

Martin, D. A. (2019). Linking fire and the United Nations sustainable development goals. *Science of the Total Environment, 662*, 547–558. https://doi.org/10.1016/j.scitotenv.2018.12.393

Matin, M. A., Chitale, V. S., Murthy, M. S., Uddin, K., Bajracharya, B., & Pradhan, S. (2017). Understanding forest fire patterns and risk in Nepal using remote sensing, geographic information system and historical fire data. *International Journal of Wildland Fire, 26*(4), 276–286. https://doi.org/10.1071/WF16056

Minuzzi, R. B., Sediyama, G. C., Barbosa, E. D. M., & Melo Júnior, J. C. F. D. (2007). Climatologia do comportamento do período chuvoso da região sudeste do Brasil. *Revista Brasileira De Meteorologia, 22*(3), 338–344. https://doi.org/10.1590/S0102-77862007000300007

Moura, C. R. W., Escobar, G. C. J., & Andrade, K. M. (2013). Padrões de circulação em superfície e altitude associados a eventos de chuva intensa na Região Metropolitana do Rio de Janeiro. *Revista Brasileira De Meteorologia, 28*, 267–280. https://doi.org/10.1590/S0102-77862013000300004

Moura, A. C. M., Freire, G. J. M., Oliveira, R. H. D., Santana, S. A. D., Pereira, M. F., Soares, A. M. E., & Voll, V. L. (2009). Geoprocessamento no Apoio a Políticas do Programa Vila Viva em Belo Horizonte-MG: Intervenções em assentamentos urbanos precários. *Revista Brasileira De Cartografia, 61*(2), 177–188.

Nimer, E. (1972). Climatologia da Região Sudeste do Brasil: Introdução à Climatologia Dinâmica - Subsídios à Geografia Regional do Brasil. *Revista Brasileira De Geografia, 34*(1), 3–48.

Nunes, J. P., Doerr, S. H., Sheridan, G., Neris, J., Santín, C., Emelko, M. B., Silins, U., Robichaud, P. R., Elliot, W. J., & Keizer, J. (2018). Assessing water contamination risk from vegetation fires: Challenges, opportunities and a framework for progress. *Hydrological Processes, 32*(5), 687–694. https://doi.org/10.1002/hyp.11434

Nunes, M. T. de O., Sousa, G. M. de, Tomzhinski, G. W., Oliveira-Júnior, J. F. de, & Couto Fernandes, M. do (2015). Variáveis Condicionantes na Susceptibilidade de Incêndios Florestais no Parque Nacional do Itatiaia. *Anuario do Instituto de Geociencias, 38*(1), 54–62. https://doi.org/10.11137/2015_1_54_62

Nuthammachot, N., & Stratoulias, D. (2021). Multi-criteria decision analysis for forest fire risk assessment by coupling AHP and GIS: Method and case study. *Environment, Development and Sustainability, 23*(12), 17443–17458. https://doi.org/10.1007/s10668-021-01394-0

Oliveira, M. T. de, & Saraiva, S. L. C. (2015). *Fundamentos de Geodésia e Cartografia: Série Tekne*. Bookman Editora.

Otto, F. E. L., Coelho, C. A. S., King, A., Perez, E. C. de, Wada, Y., van Oldenborgh, G. J., Haarsma, R., Haustein, K., Uhe, P., van Aalst, M., Aravequia, J. A., Almeida, W., & Cullen, H. (2015). Factors other than climate change, main drivers of 2014/15 water shortage in Southeast Brazil. In S. C. Herring, M. P. Hoerling, J. P. Kossin, T. C. Peterson, & P. A. Stott (Eds.). *Explaining Extreme Events of 2014 from a Climate Perspective* (vol. 96, nº12, pp. S35–S40). American Meteorological Society. https://doi.org/10.1175/BAMS-D-15-00120.1

Palm, B. B., Peng, Q., Fredrickson, C. D., Lee, B. H., Garofalo, L. A., Pothier, M. A., Kreidenweis, S. M., Farmer, D. K., Pokhrel, R. P., Shen, Y., Murphy, S. M., Permar, W., Hu, L., Campos, T. L., Hall, S. R., Ullmann, K., Zhang, X., Flocke, F., Fischer, E. V., & Thornton, J. A. (2020). Quantification of organic aerosol and brown carbon evolution in fresh wildfire plumes. *Proceedings of the National Academy of Sciences, 117*(47), 29469–29477. https://doi.org/10.1073/pnas.2012218117

Pereira, P., Bogunovic, I., Zhao, W., & Barcelo, D. (2021). Short-term effect of wildfires and prescribed fires on ecosystem services. *Current Opinion in Environmental Science & Health, 22*, 100266. https://doi.org/10.1016/j.coesh.2021.100266

Pettinari, M. L., & Chuvieco, E. (2020). Fire danger observed from space. *Surveys in Geophysics, 41*(6), 1437–1459. https://doi.org/10.1007/s10712-020-09610-8

Pigola, A., da Costa, P. R., Carvalho, L. C., Silva, L. F. D., Kniess, C. T., & Maccari, E. A. (2021). Artificial intelligence-driven digital technologies to the implementation of the sustainable development goals: A perspective from Brazil and Portugal. *Sustainability, 13*(24), 13669. https://doi.org/10.3390/su132413669

Pourghasemi, H. R., Beheshtirad, M., & Pradhan, B. (2016). A comparative assessment of prediction capabilities of modified analytical hierarchy process (M-AHP) and Mamdani fuzzy logic models using Netcad-GIS for forest fire susceptibility mapping. *Geomatics, Natural Hazards and Risk, 7*(2), 861–885. https://doi.org/10.1080/19475705.2014.984247

Prudente, T. D., & Rosa, R. (2010). Detecção de incêndios florestais no Parque Nacional da Chapada dos Veadeiros e área de entorno. *Caminhos De Geografia, 11*(35), 209–221.

Reboita, M. S., Krusche, N., Ambrizzi, T., & Rocha, R. P. D. (2012). Entendendo o Tempo e o Clima na América do Sul. *Terrae Didatica, 8*(1), 34–50. https://doi.org/10.20396/td.v8i1.8637425

Reboita, M. S., Gan, M. A., Rocha, R. P. D., & Ambrizzi, T. (2010). Regimes de precipitação na América do Sul: Uma revisão bibliográfica. *Revista Brasileira De Meteorologia, 25*, 185–204. https://doi.org/10.1590/S0102-77862010000200004

Rodrigues, J. A., Libonati, R., de Faria Peres, L., & Setzer, A. (2018). Mapeamento de áreas queimadas em Unidades de Conservação da região serrana do Rio de Janeiro utilizando o satélite Landsat-8 durante a seca de 2014. *Anuário do Instituto de Geociências, 41*(1), 318–327. https://doi.org/10.11137/2018_1_318_327

Rorig, M. L., & Ferguson, S. A. (1999). Characteristics of lightning and wildland fire ignition in the Pacific Northwest. *Journal of Applied Meteorology, 38*(11), 1565–1575. https://doi.org/10.1175/1520-0450(1999)038%3c1565:COLAWF%3e2.0.CO;2

Saaty, T. L. (1977). A scaling method for priorities in hierarchical structures. *Journal of Mathematical Psychology, 15*(3), 234–281. https://doi.org/10.1016/0022-2496(77)90033-5

Sampaio, T. V. M., & Brandalize, M. C. B. (2018). *Cartografia geral, digital e temática*. Série Geotecnologias: Teoria e prática (vol. 1). Programa de Pós-Graduação em Ciências Geodésicas. Universidade Federal do Paraná.

Santos, H. G. dos, Jacomine, P. K. T., Anjos, L. H. C. dos, Oliveira, V. A. de, Oliveira, J. B. de, Coelho, M. R., Lumbreras, J. F., & Cunha, T. J. F. (2006). *Sistema Brasileiro de Classificação de Solos*. Embrapa Solos.

Sausen, T. M., & Lacruz, M. S. P. (2015). *Sensoriamento remoto para desastres*. Oficina de Textos.

Seluchi, M. E., Beu, C. M., & Andrade, K. M. (2016). Características das Frentes Frias com Potencial para Provocar Chuvas Intensas na Região Serrana de Rio de Janeiro. *Revista Brasileira De Climatologia, 18*, 361–376. https://doi.org/10.5380/abclima.v18i0.45369

Seluchi, M. E., & Chou, S. C. (2009). Synoptic patterns associated with landslide events in the Serra do Mar, Brazil. *Theoretical and Applied Climatology, 98*(1), 67–77. https://doi.org/10.1007/s00704-008-0101-x

Silva, R. (2019). Hot spot analysis of fires in the State of Rio de Janeiro. *Geophysical Research Abstracts, EGU General Assembly, 2019*(21), 16382.

Silva, W. L., & Dereczynski, C. P. (2014). Caracterização climatológica e tendências observadas em extremos climáticos no estado do Rio de janeiro. *Anuário do Instituto de Geociências, 37*(2), 123–138. https://doi.org/10.11137/2014_2_123_138

Sivrikaya, F., & Küçük, Ö. (2022). Modeling forest fire risk based on GIS-based analytical hierarchy process and statistical analysis in Mediterranean region. *Ecological Informatics, 68*, 101537. https://doi.org/10.1016/j.ecoinf.2021.101537

Sobral, B. S., de Oliveira-Júnior, J. F., Alecrim, F., Gois, G., Muniz-Júnior, J. G., de Bodas Terassi, P. M., Pereira-Júnior, E. R., Lyra, G. B., & Zeri, M. (2020). PERSIANN-CDR based characterization and trend analysis of annual rainfall in Rio De Janeiro State, Brazil. *Atmospheric Research, 238*, 104873. https://doi.org/10.1016/j.atmosres.2020.104873

Sobral, B. S., Oliveira-Júnior, J. F., Gois, G., de Bodas Terassi, P. M., & Muniz-Júnior, J. G. R. (2018). Variabilidade espaço-temporal e interanual da chuva no estado do Rio de Janeiro. *Revista Brasileira De Climatologia, 22*, 281–308. https://doi.org/10.1016/j.atmosres.2020.104873

Srivastava, P. K., Petropoulos, G. P., Gupta, M., Singh, S. K., Islam, T., & Loka, D. (2019). Deriving forest fire probability maps from the fusion of visible/infrared satellite data and geospatial data mining. *Modeling Earth Systems and Environment, 5*(2), 627–643. https://doi.org/10.1007/s40808-018-0555-5

Tehrany, M. S., Jones, S., Shabani, F., Martínez-Álvarez, F., & Tien Bui, D. (2019). A novel ensemble modeling approach for the spatial prediction of tropical forest fire susceptibility using LogitBoost machine learning classifier and multi-source geospatial data. *Theoretical and Applied Climatology, 137*(1), 637–653. https://doi.org/10.1007/s00704-018-2628-9

Thornthwaite, C. W. (1948). An approach toward a rational classification of climate. *Geographical Review, 38*(1), 55–94. https://doi.org/10.2307/210739

Thornthwaite, C. W., & Mather, J. R. (1955). *The water balance*. Drexel Institute of Technology.

Torres, F. T. P., Ribeiro, G. A., Martins, S. V., & Lima, G. S. (2014). Mapeamento da suscetibilidade a ocorrências de incêndios em vegetação na área urbana de Ubá-MG. *Revista Árvore, 38*, 811–817. https://doi.org/10.1590/S0100-67622014000500005

UN - United Nations. (2015). *Transforming our world: The 2030 Agenda for Sustainable Development*. United Nations. Accessed 27 Oct 2021, from https://sdgs.un.org/2030agenda

UNEP - United Nations Environment Programme. (2021). *The effect of wildfires on sustainable development*. United Nations Environment Programme. Accessed 27 Oct 2021, from http://www.unep.org/news-and-stories/story/effect-wildfires-sustainable-development

USGS - United States Geological Survey. (2021). *EarthExplorer*. United States Geological Survey. Accessed 4 Aug 2021, from https://earthexplorer.usgs.gov/

van Mantgem, E. F., Keeley, J. E., & Witter, M. (2015). Faunal responses to fire in chaparral and sage scrub in California, USA. *Fire Ecology, 11*(3), 128–148. https://doi.org/10.4996/fireecology.1103128

Wei, M., Zhang, Z., Long, T., He, G., & Wang, G. (2021). Monitoring Landsat based burned area as an indicator of sustainable development goals. *Earth's Future, 9*(6), e2020EF001960. https://doi.org/10.1029/2020EF001960

Wu, C., Venevsky, S., Sitch, S., Mercado, L. M., Huntingford, C., & Staver, A. C. (2021). Historical and future global burned area with changing climate and human demography. *One Earth, 4*(4), 517–530. https://doi.org/10.1016/j.oneear.2021.03.002

Wunder, S., Calkin, D. E., Charlton, V., Feder, S., de Arano, I. M., Moore, P., Silva, F. R., & y, Tacconi, L., & Vega-García, C. (2021). Resilient landscapes to prevent catastrophic forest fires: Socioeconomic insights towards a new paradigm. *Forest Policy and Economics, 128*, 102458. https://doi.org/10.1016/j.forpol.2021.102458